RELATÓRIO DE ATIVIDADES

1 – DADOS CADASTRAIS

1.1 Nome do Beneficiário Caio Ruviaro Dantas Osório	1.2 CPF / Passaporte 022.399.050-77
1.3 Instituição Universidade Federal de Santa Maria	1.3 Programa CAPES/ nº do AUXPE CAPES/PRINT (Edital nº 41/2017) Bolsa processo nº: 88887.465639/2019-00
1.5 Projeto Recursos Energéticos	1.6 Coordenador Projeto Prof. Dr. Daniel Pinheiro Bernardon
1.7 Programa de Pós-Graduação Programa de Pós-Graduação em Engenharia Elétrica - PPGEE	

2 – BENEFÍCIO

2.1 Modalidade ( ) Missão de Trabalho (X) Bolsa Doutorado Sanduíche		
2.2 Instituição de Destino (nome da instituição e nome do centro/instituto/departamento/grupo de pesquisa) University of Oviedo (UNIOVI), Gijón, Spain Laboratory for Electrical Energy Management Unified Research (LEMUR)	2.3 Período da Atividade 2.3.1 Início 01/01/2020	2.3.2 Término 30/06/2020

3 – RECURSOS RECEBIDOS (R$)

3.1 Auxílio-deslocamento	xxxxxx
3.2 Auxílio-instalação	R$ 6.266,00 (€ 1.300,00)
3.3 Seguro-saúde	R$ 2.602,80 (6 x € 90,00 = € 540,00)
3.4 Adicional-localidade	xxxxxx
3.5 Mensalidade	R$ 40.014,00 (6 x € 1.300,00 = € 7.800,00)
3.6 Auxílio-diário	xxxxxxx

3 – DESCRIÇÃO DAS ATIVIDADES

4.1 Objetivos:

O período de Doutorado Sanduíche do aluno insere-se no contexto de formação de recursos humanos qualificados e tem como objetivo a construção de uma cooperação técnica entre a Universidade Federal de Santa Maria, a *Universidad de Oviedo* e o laboratório LEMUR, reconhecido centro de pesquisa nas áreas de sistemas de energia distribuída e sua integração na rede elétrica, incluindo o desenvolvimento de sistemas de geração, conversores de energia e estratégias de controle.

No aspecto técnico, o período de Doutorado Sanduíche do aluno teve como objetivo contribuir com o trabalho de Tese em desenvolvimento, incluindo novos cenários e aplicações de técnicas de projeto de controladores robustos e análise de estabilidade para conversores conectados à rede no contexto de microrredes e controle distribuído, o que pode fomentar novas perspectivas de pesquisa nesta área.

4.2 Atividades Realizadas:

De Janeiro a Junho de 2020, o doutorando Caio Ruviaro Dantas Osório desenvolveu parte de suas pesquisas na *Universidad de Oviedo* (UNIOVI), Gijón, Espanha, conforme previsto no Projeto de Doutorado Sanduíche intitulado "*Procedures for Robust Control Design and Stability Analysis applied to Distributed Control Systems in Power Converters*", aprovado no âmbito do Programa Institucional de Internacionalização CAPES/PrInt, do PPGEE/UFSM.

Na instituição estrangeira, o aluno participou ativamente das atividades de pesquisa do "*Laboratory for Electrical Energy Management Unified Research*" (LEMUR), sob a coorientação do Professor Pablo García Fernández, PhD.

Dentre as atividades técnicas desenvolvidas, destacam-se:

- Revisão do estado da arte com relação ao projeto de controladores robustos e análise de estabilidade aplicados a conversores conectados à rede;
- Modelagem matemática de inversores trifásicos conectados à rede por meio de filtro LCL, incluindo a obtenção de expressões analíticas de forma fechada para o cálculo dos parâmetros dos modelos discretizados;
- Obtenção de expressões analíticas para o cálculo de ganhos de realimentação de estados com base na alocação de polos do sistema em malha fechada conectado à rede;
- Desenvolvimento de controladores robustos (realimentação completa ou parcial de estados), incluindo estratégias adaptativas baseadas na identificação de parâmetros;
- Desenvolvimento de procedimentos automáticos de projeto para controladores robustos baseados em algoritmos inteligentes e metaheurísticas;
- Desenvolvimento de observadores robustos de estados para conversores conectados à rede com impedância de rede incerta, incluindo possível estratégia de adaptação do modelo da planta;
- Implementação de simulações em software especializado, para validação das estratégias estudadas;
- Programação de processador digital de sinais para implementação das estratégias de controle;
- Desenvolvimento de bancada para obtenção de resultados experimentais;
- Produção de artigos científicos e relatórios técnicos.

4.3 Resultados e/ou Impactos:

Os objetivos propostos foram atingidos.

A partir do trabalho realizado durante o Doutorado Sanduíche, verificou-se uma boa interação técnico-científica do aluno com a instituição de destino e com o coorientador no exterior. A *Universidad de Oviedo* e o LEMUR contam com uma equipe de pesquisa multidisciplinar, avançada infraestrutura laboratorial e pesquisadores com expertise no desenvolvimento de sistemas de geração distribuída baseados em fontes alternativas e sua integração com a rede elétrica. A interação com o coorientador estrangeiro contribuiu para o aumento do conhecimento do bolsista em controle aplicado a conversores conectados em rede, e no aprimoramento da metodologia de modelagem e controle que será apresentada na Tese. Desta forma, confirmou-se o bom potencial de expansão desta colaboração e a consolidação de rede de pesquisa com os pesquisadores da referida instituição estrangeira, contribuindo para a internacionalização do PPGEE/UFSM e para o aprimoramento da qualidade das produções acadêmicas deste programa de pós-graduação.

Durante o período do Doutorado Sanduíche, foi desenvolvida uma estratégia de controle robusto para inversores conectados à rede elétrica e com aplicações em microrredes, baseada na adaptação dos ganhos de realimentação de estados a partir da identificação de parâmetros do sistema, incluindo algoritmo de observação de estados para otimização do número de sensores. Desenvolveu-se também um procedimento automático de projeto de controladores PI robustos frente à incerteza paramétrica na rede elétrica, e propôs-se ainda um projeto automático, baseado em otimização, dos ganhos de realimentação de estados para conversores conectados à rede. Esta última estratégia foi confirmada experimentalmente, com resultados de acordo com exigências de norma internacional.

Até o momento, foram submetidos, com coautoria do coorientador estrangeiro, dois artigos científicos para congresso (em revisão) e está em elaboração um artigo para revista. O bolsista iniciou o desenvolvimento de uma bancada no laboratório LEMUR, para validação experimental das estratégias propostas, e o conhecimento adquirido já está sendo utilizado para a obtenção de novos resultados experimentais vinculados à tese, no laboratório GEPOC/UFSM. Mesmo sob as restrições devidas à pandemia do Covid-19, é importante ressaltar que foram obtidos resultados de muito boa qualidade, alguns dos quais são reproduzidos em anexo, fortalecendo a rede de pesquisa estabelecida com os pesquisadores da instituição estrangeira, e contribuindo para a internacionalização do PPGEE/UFSM.

Santa Maria, 21 de Agosto de 2020.

Caio Ruviaro Dantas Osório

APÊNDICE TÉCNICO

Devido ao aumento contínuo na demanda de energia, a escassez de combustíveis fósseis e a necessidade de reduzir a emissão de gases de efeito estufa, sistemas de geração baseados em fontes renováveis experimentaram um rápido desenvolvimento nas últimas décadas [1],[2]. Além disso, é crescente o interesse em sistemas de energia distribuída, permitindo assim a descentralização da geração de energia e a diversificação das fontes. Nesse sentido, conversores conectados à rede (GCCs) desempenham um papel importante, uma vez que possibilitam injetar energia de alta qualidade em redes de distribuição ou microrredes [3], [4]. Um exemplo de conversor trifásico conectado à rede por meio de filtro LCL é mostrado na Figura *1*.

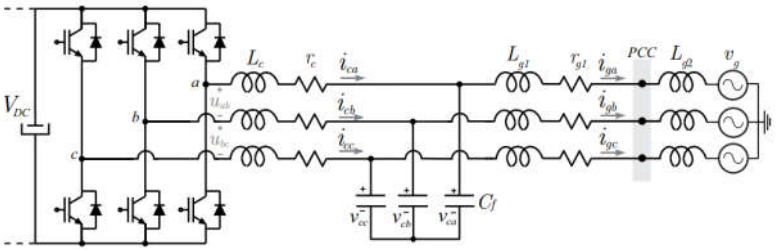

Figura 1 - Conversor trifásico conectado à rede por meio de filtro LCL

Um problema importante para o controle de corrente é lidar com a incerteza na impedância equivalente da rede no ponto de acoplamento comum (PCC), que pode variar em uma ampla faixa, deteriorando o desempenho do sistema em malha fechada, e possivelmente levando a instabilidade [5]-[7]. Este problema causa particular preocupação no cenário de geração distribuída, uma vez que tais sistemas normalmente apresentam características elétricas fracas (baixa relação de curto-circuito), uma vez que os recursos de energia renovável podem estar localizados longe da rede elétrica ou dos centros de carga [4].

Dentre as atividades desenvolvidas ao longo do período de intercâmbio, foram investigadas alternativas para o projeto analítico de controladores de corrente robustos em tempo discreto aplicado a GCCs conectados à rede elétrica por meio de filtros LCL. Expressões de forma fechada para a discretização dos modelos no referencial estacionário e para o cálculo de ganhos de realimentação de estados foram obtidas pelo Bolsista, com ajuda do coorientador estrangeiro e do orientador no Brasil. O projeto dos controladores é feito com base na alocação direta dos polos, incluindo o atraso de implementação digital e controladores ressonantes. É importante observar que a obtenção de expressões de forma fechada permite o cálculo online dos ganhos de controle, que podem ser adaptados a partir de algoritmos de identificação de parâmetros, o que confere desempenho robusto ao sistema frente a incertezas ou variações paramétrica no tempo. Ainda, para otimizar o número de sensores, algoritmos de observação de estados foram projetados.

Como exemplo de um resultado preliminar utilizando a estratégia supracitada, a Figura *2* mostra a alocação dos polos de malha fechada do sistema discretizado (filtro LCL conectado à rede, incluindo atraso de implementação digital e controlador ressonante) para diferentes valores de indutância da rede. A lei de controle por realimentação de estados é calculada a partir das medidas das correntes do lado do conversor, sendo que as tensões nos capacitores e as correntes injetadas na rede são obtidas com o algoritmo de observação de estados. Assumindo-se uma identificação precisa da impedância de rede, observa-se que o sistema de controle proposto é capaz de alocar os polos exatamente nas posições alvo (identificadas como Palvo, na Figura 2), tanto para o sistema assumindo a medição de todos os estados (medido), quanto para o sistema utilizando o observador de estados (observado).

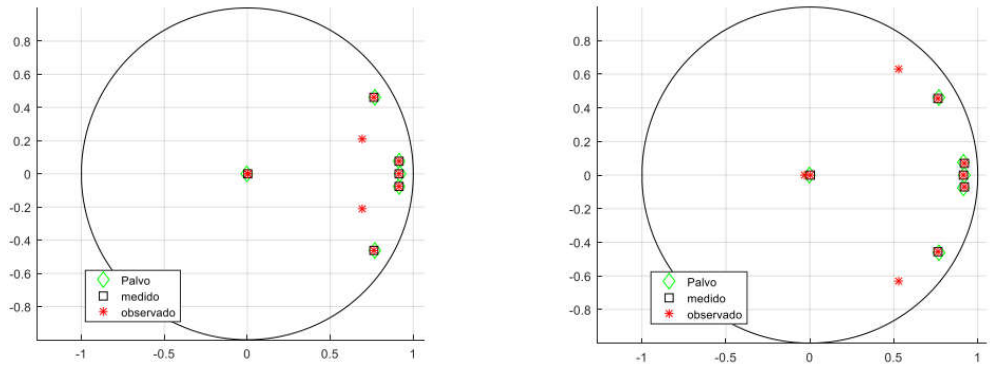

Figura 2 – Resultado da alocação de polos com a estratégia adaptativa para o cálculo dos ganhos de realimentação de estados: (a) indutância de rede igual a 8 mH; (b) indutância de rede igual a 0 mH.

Adicionalmente, foi estudada a aplicação da estratégia desenvolvida no cenário de realimentação parcial de estados, em que o projeto dos controladores é feito com base na aproximação do filtro LCL por um filtro L. Neste cenário, a ação de controle é computada com base na realimentação da corrente injetada na rede, incluindo amortecimento ativo a partir da realimentação das correntes nos capacitores do filtro. Novamente, as variáveis medidas são as correntes no filtro do lado do conversor, sendo as demais variáveis obtidas com um observador de estados. Resultados de simulação preliminares são dados na Figura *3*, em que é mostrada uma comparação entre o cenário de realimentação completa e de realimentação parcial de estados, utilizando a estratégia proposta. Verifica-se que, em ambos os cenários, foi possível recalcular os ganhos do controlador de modo a garantir estabilidade e desempenho para o conversor conectado à rede com diferentes valores de indutância.

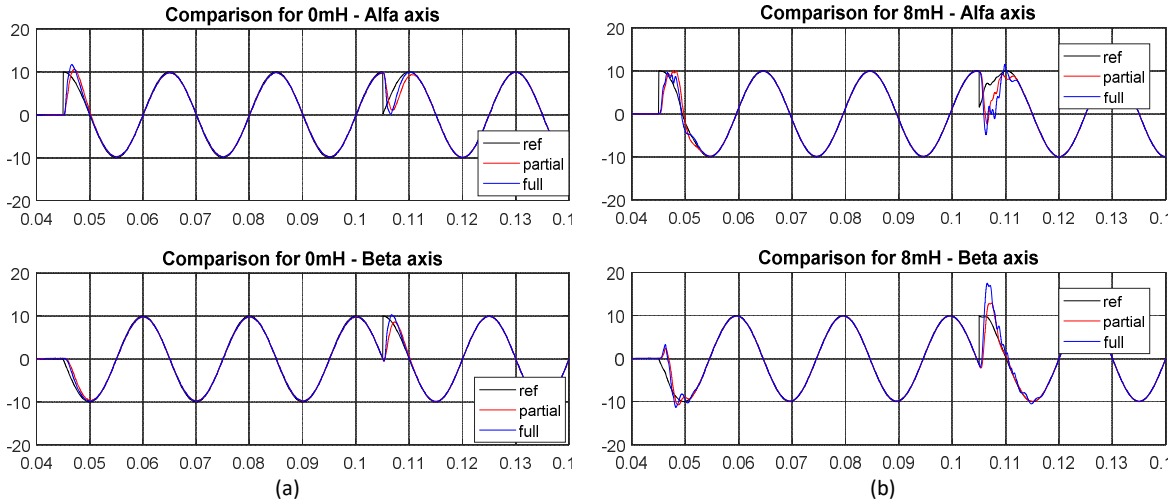

Figura 3 - Comparação entre realimentação completa e realimentação parcial de estados, considerando estratégia de adaptação dos ganhos de controle: (a) indutância de rede igual a 0 mH; (b) indutância de rede igual a 8 mH

Com relação a realimentação parcial de estados e ao projeto analítico dos ganhos de realimentação de estados nesta condição, está em revisão o artigo intitulado "*Design Procedure of Current Controllers for LCL-filtered Grid-Tied Inverters with Robust Stability Certification*", submetido ao XXIII Congresso Brasileiro de Automática. Este artigo encontra-se anexo a este documento.

Outro método importante para o controle de corrente de GCCs é o integral proporcional (PI), em que projetos convencionais são geralmente suficientes para garantir um bom desempenho em condições de rede forte e quando incertezas paramétricas não são significativas. No entanto, ao lidar com parâmetros incertos, o projeto torna-se mais desafiador, dependente de escolhas heurísticas, o que geralmente demanda uma grande quantidade de tempo em

projetos baseado em tentativa e erro [2], [3], [5]. Por este motivo, estudou-se também ao longo do intercâmbio a sintonia automática de controladores PI robustos a partir de procedimento executado offline, combinando otimização por enxame de partículas e teoremas de Kharitonov para lidar com diferentes restrições de projeto e robustez contra incertezas paramétricas. Neste tema, está em revisão o artigo intitulado "*Automatic Design of Robust Controllers for Grid-Tied Inverters based on PSO and Kharitonov's Theorem*", submetido ao XXIII Congresso Brasileiro de Automática. Este artigo encontra-se anexo a este documento.

Na Figura *4*, são apresentados exemplos de resultados de simulação em tempo real (hardware-in-the-loop) para um ensaio de variação de referência, obtidos com os controladores PI robustos projetados. É possível confirmar estabilidade robusta e desempenhos transitórios adequados para ambos os valores extremos das indutâncias da rede considerados no projeto.

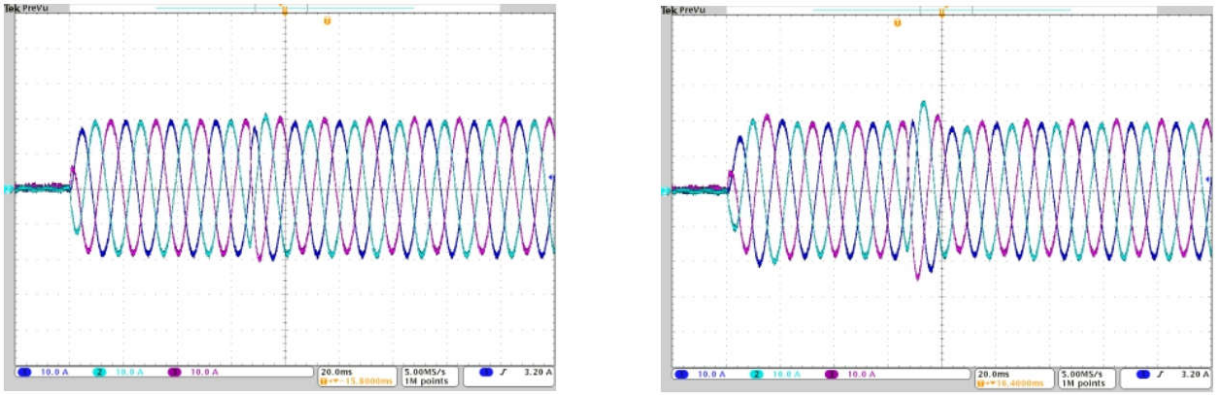

(a) (b)

Figura 4 – Respostas transitórias com os controladores PI robustos para sistema operando com indutância de rede incerta: (a) 0mH; (b) 1.5 mH.

Ainda tratando-se do desenvolvimento de procedimentos automáticos para projeto de controladores robustos, durante a realização do Doutorado Sanduíche foi apresentado no congresso *14th International Conference on Compatibility, Power Electronics and Power Engineering* o trabalho intitulado "*Robust Control of Grid-Tied Inverters using Particle Swarm Optimization and Linear Matrix Inequalities*". Este artigo fornece um procedimento de projeto para controladores de corrente robustos aplicados a inversores conectados à rede por meio de filtro LCL, adequados para a integração de fontes de energia renováveis. Um algoritmo de enxame de partículas é utilizado para encontrar ganhos de realimentação de estados a partir da otimização de uma função objetivo que permite obter um bom trade-off entre o tempo de acomodação das respostas transitórias e rejeição de distúrbios. A Figura *5* mostra resultados experimentais obtidos em protótipo para um ensaio de variação de referência da corrente injetada na rede, a partir dos quais verifica-se o bom desempenho da estratégia de projeto proposta.

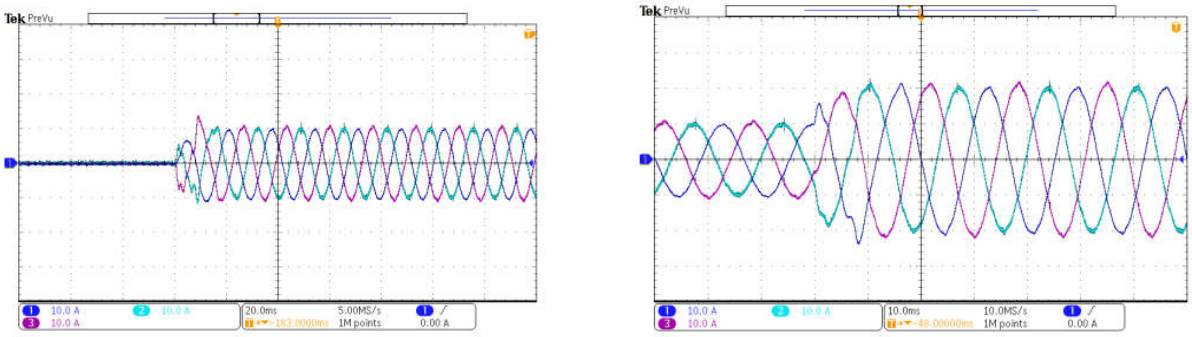

(a) (b)

Figura 5 – Resultados experimentais. Correntes trifásicas para variações de referência:
(a) partida do sistema; (b) incremento na potência ativa injetada na rede

Por fim, pode-se concluir que os resultados obtidos ao longo do Doutorado Sanduíche indicam que as estratégias propostas fornecem controladores capazes de produzir respostas transitórias e em regime permanente adequadas mesmo para conversores conectados à rede elétrica sujeitos a distúrbios e incertezas e variações paramétricas. Uma bancada experimental está sendo desenvolvida no laboratório LEMUR e, com base na boa qualidade dos resultados preliminares obtidos, há potencial para submissão de artigos de revista, como por exemplo o artigo sobre observadores robustos de estados, em construção, dado em anexo.

A Figura *6* apresenta uma parte da estrutura do laboratório LEMUR e a bancada em desenvolvimento, destinada para a validação experimental das estratégias propostas.

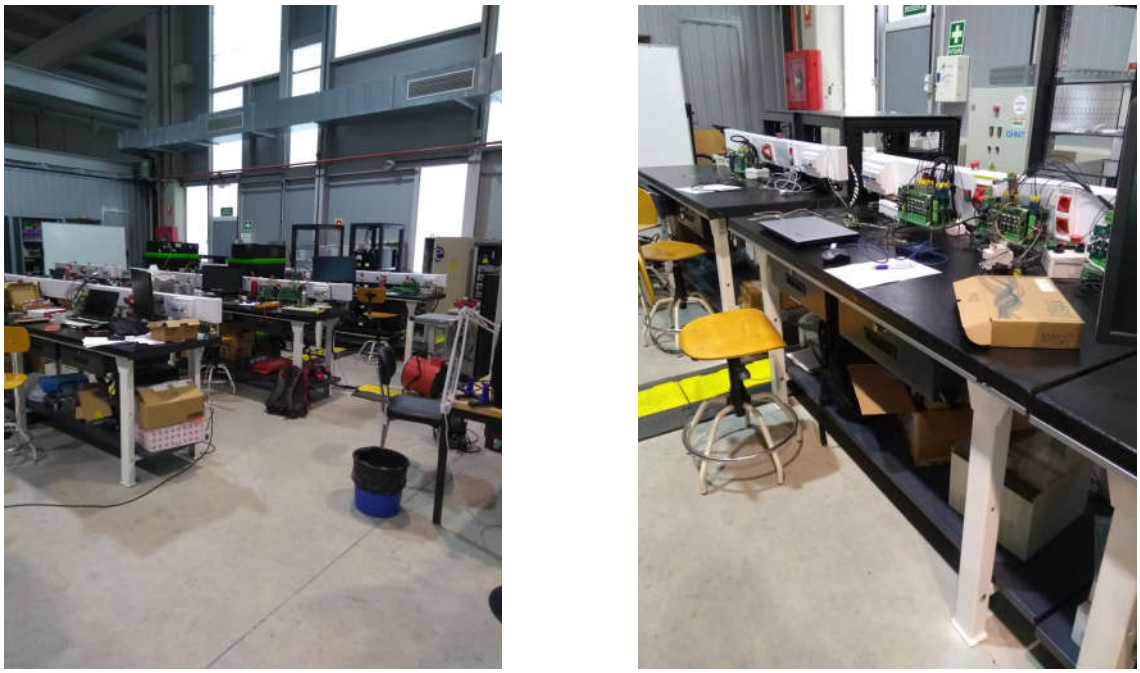

Figura 6 –Laboratório LEMUR e desenvolvimento da bancada experimental.

Referências:

[1] J. M. Guerrero et al., “Distributed Generation: Toward a New Energy Paradigm,” Ind. Electron. Mag., no. March, pp. 52–64, 2010.
[2] S. L. Lorenzen, A. B. Nielsen, and L. Bede, “Control of a grid connected converter during weak grid conditions,” 2016 IEEE 7th Int. Symp. Power Electron. Distrib. Gener. Syst. PEDG 2016, 2016.
[3] L. Tong et al., “An Improved Design of Current Controller for LCL-Type Grid-Connected Converter to Reduce Negative Effect of PLL in Weak Grid,” IEEE J. Emerg. Sel. Top. Power Electron., vol. 6, no. 2, pp. 648–663, 2017.
[4] Q. Yang et al., “Robust Current Control of Grid-tied Inverters for Renewable Energy Integration under Non-Ideal Grid Conditions,” IEEE Trans. Sustain. Energy, vol. 3029, no. c, pp. 1–1, 2019.
[5] D. Pan, C. Bao, X. Ruan, X. Wang, and W. Li, “Optimized Controller Design for LCL-Type Grid-Connected Inverter to Achieve High Robustness Against Grid-Impedance Variation,” IEEE Trans. Ind. Electron., vol. 62, no. 3, pp. 1537–1547, 2014.
[6] M. Lu, S. M. Muyeen, F. Blaabjerg, P. C. Loh, A. Al-Durra, and S. Leng, “Benchmarking of Stability and Robustness Against Grid Impedance Variation for LCL-Filtered Grid-Interfacing Inverters,” IEEE Trans. Power Electron., vol. 33, no. 10, pp. 9033–9046, 2017.
[7] J. Xu, S. Xie, B. Zhang, and Q. Qian, “Robust Grid Current Control with ImpedancePhase Shaping for LCL-Filtered Inverters in Weak and Distorted Grid,” IEEE Trans. Power Electron., vol. 33, no. 12, pp. 10240–10250, 2018.

[8] C. R. D. Osório, G. G. Koch, H. Pinheiro, R. C. L. F. Oliveira, and V. F. Montagner, V.F, "Robust current control of grid-tied inverters affected by LCL filter soft-saturation", IEEE Transactions on Industrial Electronics, 67(8), 6550-6561, 2020.
[9] L. A. Maccari, C. L. A. Santini, H. Pinheiro, R. C. L. F. Oliveira, and V. F. Montagner, V.F., "Robust optimal current control for grid-connected three-phase pulse-width modulated converters", IET Power Electronics, 8(8), 1490-1499, 2015.
[10] J. Dannehl, F. Fuchs, and P. Thøgersen, "PI state space current control of grid-connected PWM converters with LCL filters", IEEE Transactions on Power Electronics, 25(9), 2320-2330, 2010.

ANEXOS

(1) Artigo "*Design Procedure of Current Controllers for LCL-filtered Grid-Tied Inverters with Robust Stability Certification*", submetido ao XXIII Congresso Brasileiro de Automática.

(2) Artigo "*Automatic Design of Robust Controllers for Grid-Tied Inverters based on PSO and Kharitonov's Theorem*", submetido ao XXIII Congresso Brasileiro de Automática.

(3) Certificado de apresentação no congresso *14th International Conference on Compatibility, Power Electronics and Power Engineering.*

(4) Artigo "*Robust Control of Grid-Tied Inverters using Particle Swarm Optimization and Linear Matrix Inequalities*", apresentado no congresso *14th International Conference on Compatibility, Power Electronics and Power Engineering.*

(5) Primeira página do artigo sobre observadores robustos de estados, em construção para submissão em revista.

Design Procedure of Current Controllers for LCL-filtered Grid-Tied Inverters with Robust Stability Certification ⋆

Caio R. D. Osório[*,**], **Gustavo G. Koch**[*], **Pablo García**[***], **Vinicius F. Montagner**[*]

[*] *Federal University of Santa Maria, RS, Brazil*
[**] *Currently a visiting researcher at the University of Oviedo, Spain.*
[***] *Electrical Engineering Department, University of Oviedo, Spain*
(e-mail: caio.osorio@gmail.com)

Abstract: This paper proposes an alternative design procedure for current control of LCL-filtered grid-tied inverters, taking into account robustness against uncertain and possibly time-varying grid inductances. The control strategy is developed in stationary reference frame, and is based on a partial state feedback, including an active damping scheme of the LCL filter resonance. From the system parameters and the design specifications, analytical expressions for the calculation of the control gains are provided, oriented by a pole placement in discrete-time domain. These expressions are obtained neglecting the dynamics of the filter capacitor, including resonant controllers to track sinusoidal references, and taken into account the delay due to digital implementation. To certificate robust stability of the closed-loop system under time-varying grid inductances, a theoretical analysis based on a Lyapunov function is provided. Time and frequency domain results are presented for a case study, illustrating that the proposed design strategy is able to provide robust control gains leading to grid-injected currents with suitable responses for the entire range of grid inductances considered in the design.

Keywords: Active damping, direct pole placement, grid-tied inverter, LCL filter, robust control.

1. INTRODUCTION

Voltage source inverters are key elements in the integration of renewable energy sources to the electrical grid. Particularly, the current control loop plays an important role, being responsible to regulate the power flow between the source and the mains, besides ensuring grid currents with low harmonic distortion and suitable dynamics (Erickson, 1997; Blaabjerg et al., 2006; IEEE, 2018). Taking into account the switched nature of the inverter, low pass filters are required as interface between converter and grid, being the LCL filter widely used since it provides higher frequency attenuation and smaller size in comparison with the L filter (Poongothai and Vasudevan, 2019).

On the other hand, LCL filters have an intrinsic resonant behavior, which deteriorates the closed-loop performance and can lead to instability. Therefore, one important feature in the design of the current control loop is to ensure proper damping of the resonance peak, preferably by means of active damping approaches, what avoid the use of dissipative resistors (He et al., 2014). Moreover, one important challenge is to cope with uncertain and possibly time-varying grid impedances at the point of common coupling (PCC), which may also lead to poor performance or instability, for controllers designed only considering a nominal condition (García et al., 2018; Osório et al., 2020).

In this context, one important current control strategy is the state-feedback, that is proven capable of providing robustness and suitable dynamic performances for grid-tied inverter (GTI) with LCL filters subject to uncertain parameters (Gabe et al., 2009; Maccari et al., 2015; Kukkola et al., 2015; Osório et al., 2020). With this approach, internal model-based controllers can be taken into account and the closed-loop poles can be placed using different strategies, such as robust pole location (Osório et al., 2020), linear quadratic regulators (Maccari et al., 2015) or direct pole placement (Dannehl et al., 2010).

Considering the direct pole placement, one advantage is that the state-feedback gains can be calculated using closed-form analytical expressions, based on the system parameters and the control specifications (Kukkola et al., 2015). Moreover, to simplify the control design, a useful approach is to neglect the dynamics of the LCL filter capacitor, designing the controller based on an L filter approximation (Sivadas and Vasudevan, 2018). Instead of measuring all LCL filter states, this allows to compute the control law measuring, for instance, only the grid-injected currents, which reduce the number of sensor required for the implementation (Yin et al., 2013). However, this approach translates into a partial feedback of the LCL filter states, for which the stability is highly dependent on the damping of the physical system and parameter uncertain-

⋆ This study was financed in part by the Coordenação de Aperfeiçoamento de Pessoal de Nível Superior - Brasil (CAPES/PROEX) - Finance Code 001, INCT-GD, CNPq (465640/2014-1, 160884/2019-5 and 309536/2018-9), CAPES (23038.000776/2017-54), FAPERGS (17/2551-0000517-1), and CAPES-PRINT (88887.465639/2019-00).

ties. Thus, to ensure stability and suitable performance for the entire range of parameters, an additional active damping scheme must be included (Dannehl et al., 2009; García et al., 2018).

This paper provides an alternative procedure for the analytical design of discrete-time robust current controllers applied to GTIs with LCL filters. Closed-form expressions for calculating the state-feedback control gains are provided. The design relies on a direct pole placement based on an L filter approximation, which is modeled in stationary reference frame encompassing the digital implementation delay and resonant controllers. An active damping scheme based on the feedback of the capacitor current is included. The closed-loop system is designed taking into account robustness against uncertain grid inductances, and a certificate of robust stability under time-varying parameters, based on Lyapunov functions, is also provided. Simulation results in a realistic environment confirm that the proposed procedure provides controllers capable of ensuring suitable transient and steady-state responses for LCL-filtered GTIs, even when subject to uncertain and time-varying grid inductances.

2. MODELLING

A three-phase inverter connected to the grid by means of an LCL filter is shown in Figure 1. The grid impedance is assumed predominantly inductive, with an uncertain inductance L_{g2}.

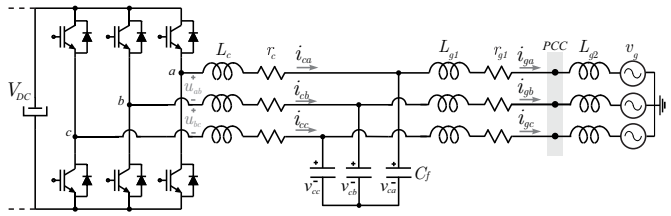

Figure 1. Three-phase LCL-filtered grid-tied inverter.

Given a balanced three-phase system, for any of the three phases, one can write that $L_g = L_{g1} + L_{g2}$, where L_g is an uncertain parameter due to the uncertainty in L_{g2}, and lies in a bounded interval given by $\mathcal{U} = [L_{gmin}, L_{gmax}]$.

Moreover, considering that there is no path for current circulation in axis-0, the topology in Figure 1 can be represented in stationary reference frame ($\alpha\beta$ coordinates) by two single-phase uncoupled systems, as depicted in Figure 2.

From Figure 2, the state-space model in stationary reference frame is given by

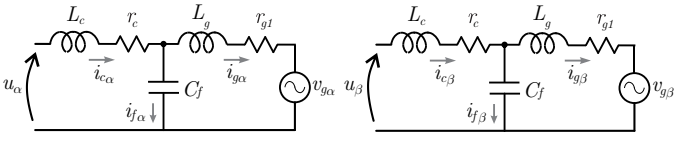

Figure 2. LCL filter model in stationary reference frame.

$$\frac{d}{dt}\begin{bmatrix} x_\alpha(t) \\ x_\beta(t) \end{bmatrix} = \begin{bmatrix} A(L_g) & 0_{3\times3} \\ 0_{3\times3} & A(L_g) \end{bmatrix}\begin{bmatrix} x_\alpha(t) \\ x_\beta(t) \end{bmatrix} + \begin{bmatrix} B_u & 0_{3\times1} \\ 0_{3\times1} & B_u \end{bmatrix}\begin{bmatrix} u_\alpha(t) \\ u_\beta(t) \end{bmatrix} + \begin{bmatrix} B_g(L_g) & 0_{3\times1} \\ 0_{3\times1} & B_g(L_g) \end{bmatrix}\begin{bmatrix} v_{g\alpha}(t) \\ v_{g\beta}(t) \end{bmatrix} \tag{1}$$

where, for the α-axis model, $x_\alpha = [i_{c\alpha}\, v_{c\alpha}\, i_{g\alpha}]'$, in which $i_{c\alpha}$ is the converter-side current, $v_{c\alpha}$ is the voltage drop across the filter capacitor and $i_{g\alpha}$ is the grid-side current. The same reasoning is valid for the β-axis model.

The matrices in (1) are given by

$$A(L_g) = \begin{bmatrix} \frac{-r_c}{L_c} & \frac{-1}{L_c} & 0 \\ \frac{1}{C_f} & 0 & -\frac{1}{C_f} \\ 0 & \frac{1}{L_g} & \frac{-r_{g1}}{L_g} \end{bmatrix},\ B_u = \begin{bmatrix} \frac{1}{L_c} \\ 0 \\ 0 \end{bmatrix},\ B_g(L_g) = \begin{bmatrix} 0 \\ 0 \\ -\frac{1}{L_g} \end{bmatrix} \tag{2}$$

Notice that under the assumption that the system is balanced, the exact same representation is obtained for the α and β axes. Thus, from this point on, these subscripts will be omitted, and the equations are valid for both axes.

For the implementation of a digital control strategy in a digital signal processor (DSP), the discretized model of the plant can be written as

$$\begin{aligned} x(n+1) &= A_d(L_g)\cdot x(n) + B_{ud}(L_g)\cdot u(n) + B_{gd}(L_g)\cdot v_g(n) \\ y(n) &= C\cdot x(n) = i_g(n), \quad C = [\,0\ 0\ 1\,] \end{aligned} \tag{3}$$

where $x(n) = [i_c(n)\, v_c(n)\, i_g(n)]'$.

From (2), for a given sampling period T_s, the matrices in (3) are given by

$$A_d(L_g) = e^{A(L_g)\cdot T_s},\ B_{ud}(L_g) = \int_0^{T_s} e^{A(L_g)\cdot\tau}\cdot B_u\cdot d\tau,$$
$$B_{gd}(L_g) = \int_0^{T_s} e^{A(L_g)\cdot\tau}\cdot B_g(L_g)\cdot d\tau \tag{4}$$

The Problem to be solved in this paper is defined as: given the LCL filter with model in (3), find a robust controller (fixed control gains) that: i) ensures stability under uncertain and possibly time-varying grid inductances; ii) ensures tracking of sinusoidal references for grid injected currents and rejection of harmonic disturbances; iii) copes with digital implementation delay of the controller.

2.1 Case Study

The system parameters for a case study are shown in Table 1, where the LCL filter parameters are borrowed from García et al. (2018). The grid inductance is defined withing a large interval to better investigate the effects of the inductance variation on the system performance.

3. PARTIAL STATE FEEDBACK CONTROL

In this Section, an analytical design procedure for a partial state feedback control is proposed. The control strategy is based on the feedback of the grid current, and the design is carried out neglecting the dynamics of the filter capacitor. Thus, the LCL filter described in (1) is approximated by

Table 1. System Parameters

Parameter	Value
L_c, C_f and L_{g1}	2.3 mH, 10 μF and 0.93 mH
r_c and r_{g1}	0.2 mΩ and 0.2 mΩ
Grid inductance L_{g2}	[0 mH, 5 mH]
DC-ling voltage (V_{DC})	400 V
Grid phase voltage	127 V(rms); 50 Hz
Sampling Frequency	16 kHz
Switching Frequency	8 kHz

an L filter, with an equivalent resistance given by $R_t = r_c + r_{g1}$, and an equivalent inductance given by $L_t = L_c + L_g$, with $L_g \in \mathcal{U}$ being an uncertain parameter.

In stationary reference frame, the dynamic equation of the three-phase L filter approximation can be written as

$$\frac{d}{dt} i_g(t) = -\frac{R_t}{L_t} i_g(t) + \frac{1}{L_t} u(t) - \frac{1}{L_t} v_g(t) \tag{5}$$

which is valid for both α and β axes.

The discretized model is given by

$$\begin{aligned} i_g(n+1) &= A_L(L_g)\cdot i_g(n) + B_{uL}(L_g)\cdot u(n) + B_{gL}(L_g)\cdot v_g(n) \\ y_L(n) &= i_g(n) \end{aligned} \tag{6}$$

where, considering a sufficiently small sampling period T_s and using, for instance, Euler Approximation, one has that $A_L = 1 - T_s R_t/L_t$, $B_{uL} = T_s/L_t$ and $B_{gL} = -T_s/L_t$.

In order to track sinusoidal grid current references and to reject disturbances from the grid voltage, consider now the inclusion of a resonant controller at a frequency ω_r. In continuous-time domain, the state-space model of this controller is given by

$$\frac{d}{dt}\begin{bmatrix}\zeta_1(t)\\ \zeta_2(t)\end{bmatrix} = \begin{bmatrix} 0 & 0 \\ -\omega_r & -2\cdot\xi_r\cdot\omega_r \end{bmatrix}\begin{bmatrix}\zeta_1(t)\\ \zeta_2(t)\end{bmatrix} + \begin{bmatrix}0\\1\end{bmatrix}(r(t) - i_g(t)) \tag{7}$$

where $\zeta_1(t)$ and $\zeta_2(t)$ are the internal states, ξ_r is the damping factor, and $r(t)$ is the reference for the grid currents.

From the discretization of (7), a state space discrete-time representation for this resonant controller is given by

$$\begin{bmatrix}\zeta_1(n+1)\\ \zeta_2(n+1)\end{bmatrix} = \begin{bmatrix} R_{11} & R_{12} \\ R_{21} & R_{22} \end{bmatrix}\begin{bmatrix}\zeta_1(n)\\ \zeta_2(n)\end{bmatrix} + \begin{bmatrix}T_1\\T_2\end{bmatrix}(r(n) - i_g(n)) \tag{8}$$

Considering now the plant in (6), the resonant controller in (8), and including a state $\phi(n)$, to represent the control delay in the digital implementation, the augmented model of the L filter approximation can be written as

$$\begin{aligned} \begin{bmatrix} i_g(n+1)\\ \phi(n+1)\\ \zeta_1(n+1)\\ \zeta_2(n+1)\end{bmatrix} &= \begin{bmatrix} A_L(L_g) & B_{uL}(L_g) & 0 & 0 \\ 0 & 0 & 0 & 0 \\ -T_1 & 0 & R_{11} & R_{21} \\ -T_2 & 0 & R_{21} & R_{22}\end{bmatrix}\begin{bmatrix} i_g(n)\\ \phi(n)\\ \zeta_1(n)\\ \zeta_2(n)\end{bmatrix} \\ &+ \begin{bmatrix}0\\1\\0\\0\end{bmatrix}u(n) + \begin{bmatrix}0\\0\\T_1\\T_2\end{bmatrix}r(n) + \begin{bmatrix}B_{gL}(L_g)\\0\\0\\0\end{bmatrix}v_g(n) \end{aligned} \tag{9}$$

which, in a more compact form, is given by

$$\begin{aligned} \rho_L(n+1) &= G_L\cdot\rho_L(n) + H_{uL}\cdot u(n) + H_{rL}\cdot r(n) + H_{gL}\cdot v_g(n) \\ y(n) &= C_L\cdot\rho_L(n) = i_g(n), \;\; C_L = [\,1\;0\;0\;0\,] \end{aligned} \tag{10}$$

3.1 Control Design - Feedback of the Grid-Side Current

Based on the L filter approximation in (10), consider the state-feedback control law given by

$$u_L(n) = -K_L\cdot\rho_L(n) = -\,[\,k_{ig}\;\; k_d\;\; k_{r1}\;\; k_{r2}\,]\begin{bmatrix} i_g(n)\\ \phi(n)\\ \zeta_1(n)\\ \zeta_2(n)\end{bmatrix} \tag{11}$$

Replacing the control law (11) in (10) leads to the closed-loop system

$$\rho_L(n+1) = (G_L - H_{uL}\cdot K_L)\,\rho_L(n) + H_{rL}\cdot r(n) + H_{gL}\cdot v_g(n) \tag{12}$$

From (12), considering the grid-voltage as an external disturbance and making $v_g(n) = 0$, the transfer function from the reference $r(n)$ to the output $i_g(n)$ can be written as

$$\frac{i_g(z)}{r(z)} = C_L(z\cdot I - (G_L - H_{uL}\cdot K_L))^{-1} H_r \tag{13}$$

where the characteristic polynomial (i.e., the denominator) is given by

$$P_L(z) = \det(z\cdot I - G_L + H_{uL}\cdot K_L) \tag{14}$$

Notice that, for time-invariant systems with precisely known parameters, if the system is controllable, a gain vector K_L can be calculated such that $P_L(z)$ is equal to a target characteristic polynomial, given by

$$\begin{aligned} Q(z) &= (z-\delta_1)(z-\delta_2)(z-\delta_3)(z-\delta_4) \\ &= z^4 + Q_3 z^3 + Q_2 z^2 + Q_1 z + Q_0 \end{aligned} \tag{15}$$

This polynomial $Q(z)$ allocates the closed-loop poles in arbitrary positions defined by the designer (i.e., δ_1, δ_2, δ_3 and δ_4), setting the desired closed-loop dynamics.

To accomplish that, the gain vector K_L can be calculate using numerical tools, such as the command *place*, in MATLAB. On the other hand, analytical expressions for the gains computation is a matter of interest, since enable, for instance, on-line computation of the gains, useful in adaptive control strategies.

One efficient way to provide closed-form expressions for the calculation of K_L is using Ackermann's formula (Dorf and Bishop, 2008). For the particular fourth-order system in (9)-(10), the gain vector K_L is given by

$$K_L = \mathcal{M}\cdot\mathcal{C}^{-1}\cdot\psi \tag{16}$$

where,

$$\begin{aligned} &\mathcal{M} = [\,0\;0\;0\;1\,] \\ &\mathcal{C} = \left[\,H_{uL}\;\; G_L\cdot H_{uL}\;\; {G_L}^2\cdot H_{uL}\;\; {G_L}^3\cdot H_{uL}\,\right] \\ &\psi = {G_L}^4 + Q_3\cdot{G_L}^3 + Q_2\cdot{G_L}^2 + Q_1\cdot G_L + Q_0\cdot I \end{aligned} \tag{17}$$

with G_L and H_{uL} given in (10), and Q_3, Q_2, Q_1 and Q_0 being the coefficients of the desired characteristic polynomial, as given in (15).

The closed-form analytical expressions for the calculation of the gains are given in Appendix A.

Remark 1: Notice that $\mathcal{C}$ is the controlability matrix of the system (10). Thus, if the system is controllable, $\mathcal{C}$ is invertible and there is a gain vector K_L that allocate the closed-loop poles as defined by the desired characteristic polynomial. On the other hand, although the closed-loop

poles can be set arbitrarily, due to constrains such as control saturation and limited bandwidth, there is no guarantee that the resulting gain K_L would lead to a control action viable in practice. Thus, a tradeoff between dynamic performance and control effort must be taken into account when choosing the poles location.

Remark 2: The design of fixed control gains will be investigated here, and not an adaptive strategy. In this context, since the grid inductances are assumed to be uncertain parameters, it is not possible to place the poles in the exact same positions for the entire range of parameters, and a nominal condition must be chosen to design the control gains. Thus, a trade-off between robustness and dynamic performance must also be taken into account when choosing the poles location.

Based on what was stated in the *Remark 1*, Subsection 3.2 provides a procedure for the choice of the pole location.

Considering what was stated in *Remark 2*, it is proposed here to design the controller for a nominal condition given by $L_g = L_{gmin}$. Although the controller is being designed using an L filter approximation, the actual application is the LCL filter depicted in Figure 1. In this way, considering the LCL resonance frequency, the minimum grid inductance represents the condition with higher resonance frequency.

3.2 Criteria for Pole Location

Based on the L filter approximation, to define the closed-loop poles location of the system (10), the following strategy is proposed here:

i) In continuous-time, consider that a pair of complex poles is chosen to set the dominant dynamics of the closed-loop system, given by

$$s^2 + 2\cdot\xi_{dom}\cdot\omega_{dom}\cdot s + {\omega_{dom}}^2 \tag{18}$$

The parameter ξ_{dom} is the damping ratio, and can be set close to 1 in order to avoid oscillations or large overshoots. Parameter ω_{dom} can be chosen based on the desired bandwidth of the system. After defining the desired dynamics, the discrete poles are given by

$$\delta_{1,2} = e^{\left(-\xi_{dom} \pm j\sqrt{1-{\xi_{dom}}^2}\right)\cdot\omega_{dom}\cdot T_s} \tag{19}$$

Notice that if $\delta_{1,2}$ are the dominant poles, then the modulus $|\delta_{1,2}|$ defines a limitation for the decay ratio of the closed-loop transient responses.

ii) The third pole is set to $\delta_3 = 0$, originated from the delay due to the digital implementation.

iii) The fourth pole, δ_4, is set as a real pole, with a value slightly lower than the modulus $|\delta_{1,2}|$. This choice avoid higher control gains, but also keeping the limit for the decay ratio of the closed-loop transient responses given by $\delta_{1,2}$.

Considering the case study with parameters in Table 1, model in (10) is computed for $L_{g2} = 0$ mH and including a resonant controller tuned at 50 Hz, with a damping factor of 0.0001.

Following the steps provided in Section 3.2, the pole location is defined for $\omega_{dom} = 350$ Hz and $\xi_{dom} = 0.9$, leading to $\delta_{1,2} = 0.882059 \pm j\ 0.052908$, $\delta_3 = 0$ and $\delta_4 = 0.88$. Given these poles, the coefficients of the characteristic polynomial (Q_3, Q_2, Q_1, Q_0) are obtained from (15), and then the control gains are computed using the equations (A.1)-(A.4), in the Appendix, leading to

$$K_L = [\,20.132019\ \ 0.347752\ \ 153.276571\ \ 147.154611\,] \tag{20}$$

For a sweep in the uncertain parameter L_g, from $L_{gmin} = 0.93$ mH to $L_{gmax} = 5.93$ mH, Figure 3 shows the closed-loop poles of the L filter approximation in (10), with controller (11) and gains in (20). All poles are inside the unit circle, indicating stability for the entire range of parameters. Moreover, the desired pole location is depicted by red squares. When the design condition matches the uncertain parameter (i.e. $L_g = L_{gmin}$), the poles are allocated exactly at the desired positions. As the actual value of L_g diverges from the nominal condition, the poles are shifted towards the edge of the unit circle, which tends to reduce the dynamic performance.

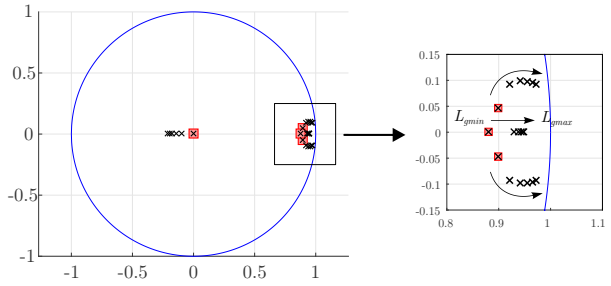

Figure 3. Closed-loop poles for a sweep in L_g: L filter approximation (10), with control law (11) and gains in (20).

It is important to mention that the choices of the pole location for this case study were made considering a trade-off between robustness and performance under uncertain grid inductances, for the interval given in Table 1. If this interval had closer bounds or, ideally, if the grid inductance was precisely known, the specifications could be improved to achieve higher dynamic performance.

4. RESPONSES OF THE LCL FILTER WITH PARTIAL STATE FEEDBACK CONTROLLER

The control design procedure in Section 2 is based on an L filter approximation. Therefore, in this section, the responses of the actual LCL filter will be evaluated.

From the model in (3) and considering the control law (11), the augmented closed-loop system of the LCL filter, including the resonant controller and the digital implementation delay, is given by

$$\begin{bmatrix} x(n+1) \\ \phi(n+1) \\ \zeta_1(n+1) \\ \zeta_2(n+1) \end{bmatrix} = \begin{bmatrix} A_d(L_g) & B_{ud}(L_g) & 0_{3\times1} & 0_{3\times1} \\ K_x & -k_d & -k_{r1} & -k_{r2} \\ -T_1\cdot C & 0 & R_{11} & R_{12} \\ -T_2\cdot C & 0 & R_{21} & R_{22} \end{bmatrix} \begin{bmatrix} x(n) \\ \phi(n) \\ \zeta_1(n) \\ \zeta_2(n) \end{bmatrix} + \begin{bmatrix} 0_{3\times1} \\ 0 \\ T_1 \\ T_2 \end{bmatrix} r(n) + \begin{bmatrix} B_{gd}(L_g) \\ 0 \\ 0 \\ 0 \end{bmatrix} v_g(n) \tag{21}$$

where $x(n) = [i_c(n)\, v_c(n)\, i_g(n)]'$ and $K_x = [\,0\ 0\ k_{ig}\,]$.

Given the model (21), with parameters from the case study (Table 1) and control gains in (20), Figure 4 shows the closed-loop poles for a sweep in the uncertain parameter L_g, from L_{gmin} to L_{gmax}. This figure shows that when the actual LCL filter is taken into account, the poles related to the inherent resonance of the filter are placed outside the unit circle, leading to an unstable closed-loop system.

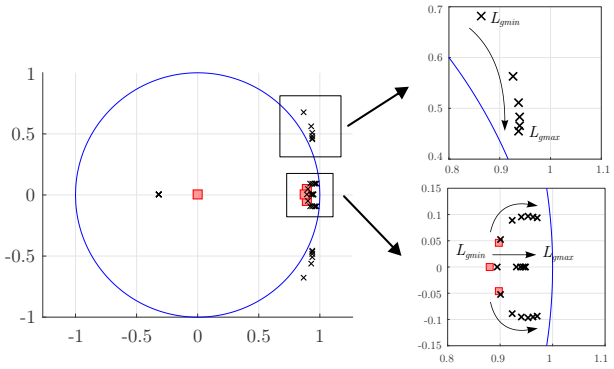

Figure 4. Closed-loop poles for a sweep in L_g: LCL filter model in (21), with control gains in (20).

This behavior is expected since the control design was based on an L filter approximation. When the grid-side current is the only state of the LCL filter being feedback, a damping strategy is usually required to enable stable operation with suitable dynamics under the LCL resonance.

4.1 Modified Control Law - Active Damping

To provide active damping of the LCL filter resonance, consider the feedback of the capacitor current i_f, given by

$$u_{ad}(n) = k_{ad} \cdot i_f(n) = k_{ad} \cdot (i_c(n) - i_g(n)) \tag{22}$$

where u_{ad} is an additional parcel of the control law, related to the active damping, and k_{ad} is the respective gain.

From the control law (11), but now including the active damping in (22), one has that the modified control law applied to the LCL filter is given by

$$u_{LCL}(n) = u_L(n) + u_{ad}(n) \tag{23}$$

The closed-loop system considering the model in (21) and the modified control law in (23) is given by

$$\begin{bmatrix} x(n+1) \\ \phi(n+1) \\ \zeta_1(n+1) \\ \zeta_2(n+1) \end{bmatrix} = \begin{bmatrix} A_d(L_g) & B_{ud}(L_g) & 0_{3\times1} & 0_{3\times1} \\ K_m & -k_d & -k_{r1} & -k_{r2} \\ -T_1 \cdot C & 0 & R_{11} & R_{12} \\ -T_2 \cdot C & 0 & R_{21} & R_{22} \end{bmatrix} \begin{bmatrix} x(n) \\ \phi(n) \\ \zeta_1(n) \\ \zeta_2(n) \end{bmatrix} + \begin{bmatrix} 0_{3\times1} \\ 0 \\ T_1 \\ T_2 \end{bmatrix} r(n) + \begin{bmatrix} B_{gd}(L_g) \\ 0 \\ 0 \\ 0 \end{bmatrix} v_g(n) \tag{24}$$

where

$$K_m = [\, k_{ad} \quad 0 \quad -(k_{ig} + k_{ad}) \,]$$

and the gains k_{ig}, k_d, k_{r1} and k_{r2} are designed with the procedure proposed in Section 3.

System (24) can be written in a more compact form as

$$\begin{aligned} \rho(n+1) &= G_{\text{mf}}(L_g) \cdot \rho(n) + H_r \cdot r(n) + H_g \cdot v_g(n) \\ y(n) &= C_{aug} \cdot \rho(n) = i_g(n), \quad C_{aug} = [\, 0 \; 0 \; 1 \; 0 \; 0 \; 0 \,] \end{aligned} \tag{25}$$

The design of the active damping gain can be done by analysing the closed-loop poles of the system (24), for different choices of k_{ad}.

Considering the proposed control design strategy, the damping gain should be negative in order to have stable operation. Moreover, the modulus of k_{ad} must be large enough so that all closed-loop poles remain inside the unit circle for the entire range of $L_g \in \mathcal{U}$. On the other hand, a limitation on the modulus of k_{ad} must be considered in order to minimize the control effort, since increasing excessively its modulus leads to an increase in the natural frequency of the filter resonance.

Taking into account these considerations, the active damping gain chosen for the case study with parameters in Table 1 is given by

$$k_{ad} = -20 \tag{26}$$

Considering (24), with control gains in (20) and damping gain in (26), the closed-loop poles of the system is shown in Figure 5, for a sweep in the uncertain parameter L_g, from L_{gmin} to L_{gmax}. Differently from Figure 4, all closed-loop poles are now inside the unit circle, indicating stability for the entire range of L_g.

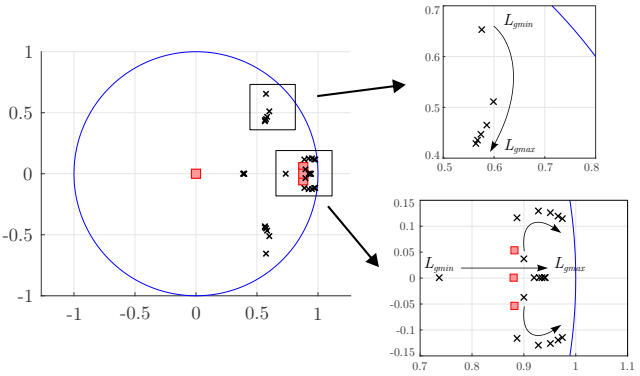

Figure 5. Closed-loop poles for a sweep in L_g: LCL filter model (24), with control gains in (20) and (26).

To confirm the capacity of this closed-loop system to track sinusoidal references, Figure 6(a) shows the frequency responses from the reference to the output, for a sweep in L_g, from L_{gmin} to L_{gmax}. It possible to verify gain equal to 0 dB at the frequency $2\pi50$ rad/s, which ensures tracking of sinusoidal references at this frequency. The capacity to reject disturbances from the grid voltage is confirmed in the Bode diagram show in Figure 6(b), where it possible to verify attenuation in the entire frequency range.

Figure 7(a) and (b) show the closed-loop responses for a reference variation test performed with the extreme values of the uncertain parameter. It is possible to verify that the closed-loop system is able to track the grid current reference with suitable transient and steady state performances, for both extreme values of the grid inductance.

Remark 3: Notice that the design of k_{ad} relies on the desired pole location, as defined in Section 3.2. If the desired pole location impairs the design of a suitable active damping (i.e. if it is not possible to stabilize the system for the entire range of parameters), thus the tradeoff between robustness and performance must be reconsidered, and

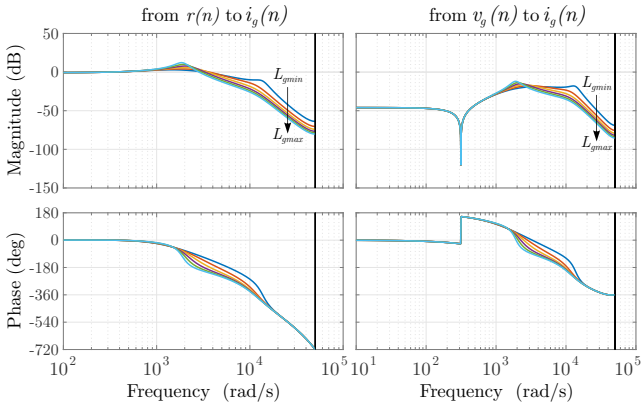

(a) (b)

Figure 6. Closed-loop frequency responses for a sweep in L_g: (a) from the reference to the output; (b) from the disturbance to the output.

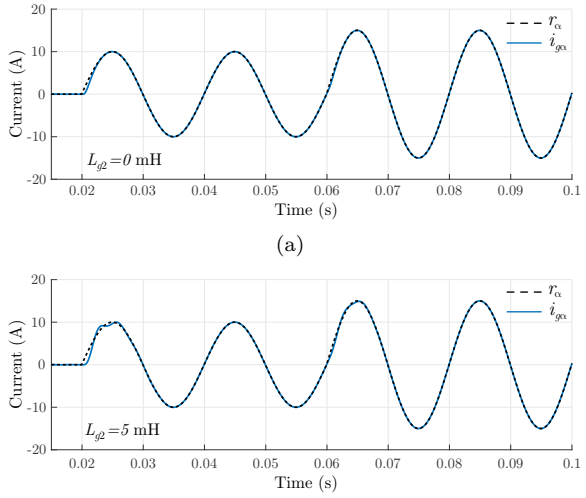

(a)

(b)

Figure 7. Closed-loop responses for a reference variation test with: (a) $L_{g2} = 0$ mH; (b) (a) $L_{g2} = 5$ mH

the pole location must be relaxed by reducing the desired bandwidth or the damping of the system.

Remark 4: Notice that for the computation of (23), besides the grid-side current (i_g), the only additional state required is the converter-side (i_c) current, which is reasonable considering that this measurement is usually available in industrial inverters for protection purposes. Thus, the control strategy presented in Section 3 requires less sensors then a full state feedback control, demanding the same amount of measurements then a classical PI controller with the same active damping scheme.

5. CERTIFICATE OF ROBUST STABILITY UNDER TIME-VARYING PARAMETERS

The analysis of the closed-loop poles shown in Figure 5 provides a robust stability indicative for the system in (24)–(25), taking into account uncertain but time-invariant grid inductances. In this context, it is important to provide a theoretical certificate of stability valid for any value of L_g lying in a given bounded interval, encompassing arbitrarily fast variation of this parameter over time.

The stability of the closed-loop system (25) can be analyzed by means of the asymptotic stability of the polytopic system given by (Boyd et al., 1994)

$$\rho(n+1) = G_{\text{mf}}(\theta(n))\cdot\rho(n), \tag{27}$$

with

$$G_{\text{mf}}(\theta(n)) = \theta(n)\cdot G_{\text{mf1}} + (1-\theta(n))\cdot G_{\text{mf2}} \tag{28}$$

for all real values of $\theta(n)$, with $0 \leq \theta(n) \leq 1$, and vertices given by

$$G_{\text{mf1}} = G_{\text{mf}}(L_{gmin}) \quad \text{and} \quad G_{\text{mf2}} = G_{\text{mf}}(L_{gmax}) \tag{29}$$

The time-variant system (27) is asymptotically stable if there is a matrix $P = P' > 0$, such that

$$G_{\text{mf}i}{}'\cdot P\cdot G_{\text{mf}i} - P < 0, \quad \text{for} \quad i = 1, 2 \tag{30}$$

This result is based on a Lyapunov function given by $v(\rho(n)) = \rho(n)'\cdot P\cdot\rho(n)$, which certifies the stability of the closed-loop system for slow or arbitrary fast parametric variations over time.

For the case study, verifying the feasibility of (30) for the vertices (29) and gains in (20) and (26), there is solution P for the problem with $L_{g2} \in [0$ mH, 4.7 mH], which certifies closed-loop stability for uncertain but also time-variant grid inductances lying in this interval.

6. RESULTS

The results shown in this section were obtained using the software PSIM. The LCL-filtered grid-tied inverter depicted in Figure 1 was simulated with the parameters on Table 1. The control algorithm was written in C language, with syntax compatible with DSP implementation. The converter-side and grid-side currents are measured (*abc* coordinates) and, after analog to digital conversion, are transformed to $\alpha\beta$ coordinates using the Clarke transformation. The control law is digitally implemented based on (23), with gains in (20) and (26). A space vector modulation is used to drive the inverter switches. The synchronism of the grid currents with voltage ate the point of common coupling (PCC) is ensured by a Kalman Filter algorithm (Cardoso et al., 2008).

To verify the closed-loop performance subject to uncertain grid inductances, tests under grid current reference variations are performed. Considering injection of active power into the grid, in the instant $t = 0.02$ s, the reference is changed from 0 A to 10 A (peak), and in $t = 0.06$ s the reference is changed from 10 A to 20 A (peak). Figure 8 shows the current-responses in $\alpha\beta$ coordinates for the system operating with L_{gmin} (i.e. $L_{g2} = 0$ mH), while Figure 9 shows the current-responses with L_{gmax} (i.e. $L_{g2} = 5$ mH).

Figure 8 and Figure 9 confirm stable responses for both extreme values of the grid inductance, with overall suitable transient and steady state performances as expected by the analysis of the closed-loop poles in Figure 5 and the frequency responses in Figure 6. When compared to the nominal condition chosen for the design (L_{gmin}), the closed-loop responses with the maximum grid inductance exhibit a deteriorated transient performance. This outcome is expected in view of the need to guarantee robustness with fixed gains for a wide range of parameters.

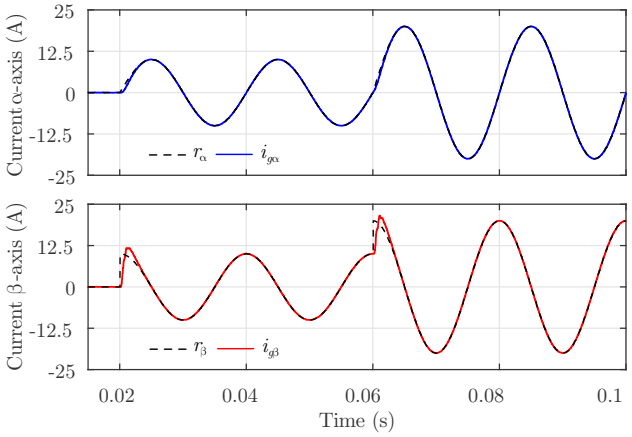

Figure 8. Currents in α-axis (top) and β-axis (bottom) for a reference variation test with $L_{g2} = 0$ mH.

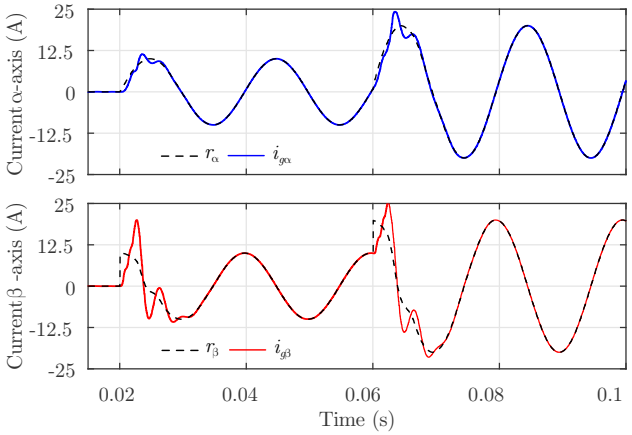

Figure 9. Currents in α-axis (top) and β-axis (bottom) for a reference variation test with $L_{g2} = 5$ mH.

Figure 10(a) and (b) show the three-phase grid currents in *abc* coordinates with respect to the $\alpha\beta$ currents shown in Figure 8 and Figure 9, respectively. These results confirm that the proposed control design leads to a robust closed-loop system, with suitable transient and steady state performances for the entire range of parameters.

The analysis presented in Section 5 certifies robust stability against arbitrarily fast variation of the grid inductance, lying in the interval [0 mH, 4.7 mH]. To confirm that, Figure 11 shows the responses of the grid currents, in $\alpha\beta$ coordinates, under switching of the grid inductance from 0 mH to 4.7 mH, at $t = 0.05$ s, and from 4.7 mH to 0 mH, at $t = 0.08$ s.

Figure 12 shows the three-phase grid currents, in *abc* coordinates, with respect to the $\alpha\beta$ currents shown in Figure 11. This results confirm stability under time-varying parameters, with suitable transient and steady-state responses.

7. CONCLUSION

This paper proposed a design procedure of current controllers applied to LCL-filtered grid-tied inverters. The procedure is based on analytical expressions for calculation of the control gains, ensuring suitable closed-loop pole

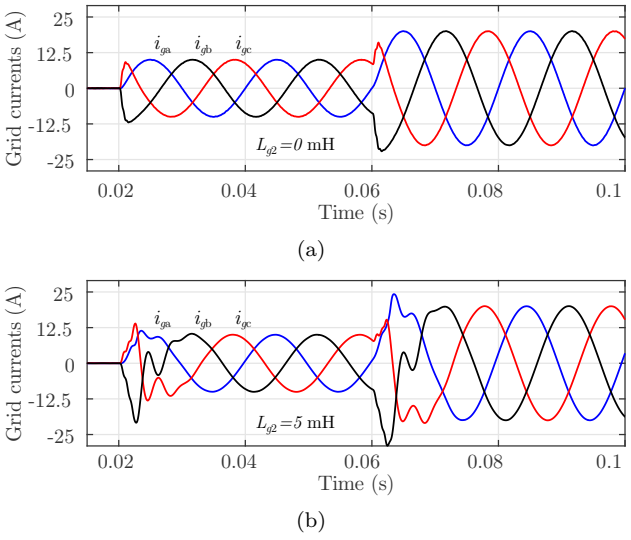

Figure 10. Three-phase grid currents for the reference variation test with: (a) $L_{g2} = 0$ mH; (b) $L_{g2} = 5$ mH.

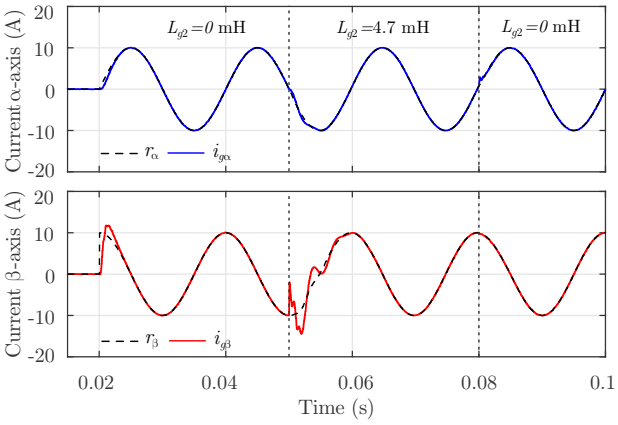

Figure 11. Currents in α-axis (top) and β-axis (bottom) under switching of the grid inductances.

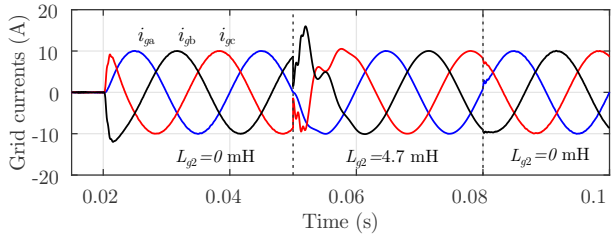

Figure 12. Three-phase grid currents under switching of the grid inductances.

location in discrete-time domain, encompassing the delay in digital control implementation, resonant controllers and operation with uncertain grid inductances. The stability of the closed-loop system against time-varying parameters is ensured by linear matrix inequalities, based on a Lyapunov function. The control gains obtained with the proposed procedure are evaluated in PSIM simulations, ensuring good performances for the closed-loop systems. One advantage of the direct pole placement is that the state-feedback gains can be calculated in an efficient way, from the system parameters and the control specifications, using closed-form analytical expressions. This enables, for

instance, automatic tuning of the controllers and, also online adaptation of the gains, which is an interesting feature to be explored in future works.

REFERENCES

Blaabjerg, F., Teodorescu, R., Liserre, M., and Timbus, A. (2006). Overview of control and grid synchronization for distributed power generation systems. *IEEE Transactions on Industrial Electronics*, 53(5), 1398 –1409.

Boyd, S., El Ghaoui, L., Feron, E., and Balakrishnan, V. (1994). *Linear Matrix Inequalities in System and Control Theory*. SIAM Studies in Applied Mathematics, Philadelphia, PA.

Cardoso, R., de Camargo, R.F., Pinheiro, H., and Gründling, H.A. (2008). Kalman filter based synchronisation methods. *IET Generation, Transmission Distribution*, 2(4), 542–555.

Dannehl, J., Fuchs, F., and Thøgersen, P. (2010). PI state space current control of grid-connected PWM converters with LCL filters. *IEEE Transactions on Power Electronics*, 25(9), 2320 –2330.

Dannehl, J., Wessels, C., and Fuchs, F. (2009). Limitations of voltage-oriented PI current control of grid-connected PWM rectifiers with filters. *IEEE Transactions on Industrial Electronics*, 56(2), 380 –388.

Dorf, R.C. and Bishop, R.H. (2008). *Modern control systems*. Prentice Hall, Upper Saddle River, USA, 11 edition.

Erickson, R.W. (1997). *Fundamentals of Power Electronics*. Chapman & Hall, New York, NY.

Gabe, I.J., Montagner, V.F., and Pinheiro, H. (2009). Design and implementation of a robust current controller for VSI connected to the grid through an LCL filter. *IEEE Transactions on Power Electronics*, 24(6), 1444–1452.

García, P., Sumner, M., Navarro-Rodríguez, ., Guerrero, J.M., and García, J. (2018). Observer-based pulsed signal injection for grid impedance estimation in three-phase systems. *IEEE Transactions on Industrial Electronics*, 65(10), 7888–7899.

He, Y., Wang, K., and Chung, H.S. (2014). Utilization of proportional filter capacitor voltage feedforward to realize active damping for digitally-controlled grid-tied inverter operating under wide grid impedance variation. In *2014 IEEE Energy Conversion Congress and Exposition (ECCE)*, 4450–4457.

IEEE (2018). IEEE standard for interconnection and interoperability of distributed energy resources with associated electric power systems interfaces. *IEEE Std 1547-2018 (Revision of IEEE Std 1547-2003)*, 1–138.

Kukkola, J., Hinkkanen, M., and Zenger, K. (2015). Observer-based state-space current controller for a grid converter equipped with an LCL filter: Analytical method for direct discrete-time design. *IEEE Transactions on Industry Applications*, 51(5), 4079–4090.

Maccari, L.A., Santini, C.L.A., Pinheiro, H., Oliveira, R.C.L.F., and Montagner, V.F. (2015). Robust optimal current control for grid-connected three-phase pulse-width modulated converters. *IET Power Electronics*, 8(8), 1490–1499.

Osório, C.R.D., Koch, G.G., Pinheiro, H., Oliveira, R.C.L.F., and Montagner, V.F. (2020). Robust current control of grid-tied inverters affected by LCL filter soft-saturation. *IEEE Transactions on Industrial Electronics*, 67(8), 6550–6561.

Poongothai, C. and Vasudevan, K. (2019). Design of LCL filter for grid-interfaced pv system based on cost minimization. *IEEE Transactions on Industry Applications*, 55(1), 584–592.

Sivadas, D. and Vasudevan, K. (2018). Stability analysis of three-loop control for three-phase voltage source inverter interfaced to the grid based on state variable estimation. *IEEE Transactions on Industry Applications*, 54(6), 6508–6518.

Yin, J., Duan, S., and Liu, B. (2013). Stability analysis of grid-connected inverter with LCL filter adopting a digital single-loop controller with inherent damping characteristic. *IEEE Transactions on Industrial Informatics*, 9(2), 1104–1112.

Appendix A. ANALYTICAL EXPRESSIONS FOR CONTROL GAIN VECTOR COMPUTATION

From the Ackermann's formula, solving (16), the closed-form analytical expressions for the computation of the entries of the vector K_L, in (11), are given by

$$k_{ig} = \frac{Q_2 + Q_3\left(A_{dL} + f_0\right) + {A_{dL}}^2 + A_{dL} f_0 + f_2 + f_4 + {R_{11}}^2 + {R_{22}}^2}{B_{udL}} \tag{A.1}$$

$$k_d = Q_3 + A_{dL} + R_{11} + R_{22} \tag{A.2}$$

$$k_{r1} = \frac{a_0 Q_0 + a_1 Q_1 + a_2 Q_2 + \left(a_{3a} + a_{3b}\right) Q_3 + \left(a_{4a} + a_{4b}\right) Q_4}{a_{div}} \tag{A.3}$$

$$k_{r2} = \frac{b_0 Q_0 + b_1 Q_1 + b_2 Q_2 + \left(b_{3a} + b_{3b}\right) Q_3 + \left(b_{4a} + b_{4b}\right) Q_4}{b_{div}} \tag{A.4}$$

with auxiliary parameters given by

$$\begin{aligned} &f_0 = R_{11} + R_{22},\ f_1 = R_{11}R_{21},\ f_2 = R_{12}R_{21},\ f_3 = R_{21}R_{22} \\ &f_4 = R_{11}R_{22},\ f_5 = R_{11}R_{12},\ f_6 = R_{12}R_{22} \end{aligned} \tag{A.5}$$

The parameters for the calculation of k_{r1}, in (A.3), are given by

$$\begin{aligned} a_0 &= -T_2, \\ a_1 &= T_1 R_{21} - T_2 R_{11}, \\ a_2 &= T_1\left(f_1 + f_3\right) - T_2\left({R_{11}}^2 + f_2\right), \\ a_{3a} &= T_1\left(f_1 f_0 + f_3 R_{22} + f_2 R_{21}\right), \\ a_{3b} &= -T_2\left({R_{11}}^3 + 2 f_1 R_{12} + f_2 R_{22}\right), \\ a_{4a} &= T_1\left(f_1 + f_3\right)\left({R_{11}}^2 + 2 f_2 + {R_{22}}^2\right), \\ a_{4b} &= -T_2\left(R_{12} f_4\left(f_1 + f_3\right) + \left({R_{11}}^2 + f_2\right)^2\right), \\ a_{div} &= B_{udL}\left(R_{12}{T_2}^2 - R_{21}{T_1}^2 + R_{11}T_1T_2 - R_{22}T_1T_2\right) \end{aligned} \tag{A.6}$$

and the parameters for the calculation of k_{r2}, in (A.4), are given by

$$\begin{aligned} b_0 &= T_1, \\ b_1 &= T_1 R_{22} - T_2 R_{12}, \\ b_2 &= T_1\left({R_{22}}^2 + f_2\right) - T_2\left(f_5 + f_6\right), \\ b_{3a} &= T_1\left({R_{22}}^3 + 2 f_2 R_{22} + f_1 R_{12}\right), \\ b_{3b} &= -T_2\left(f_5 R_{11} + 2 f_5 R_{22} + f_2 R_{12}\right), \\ b_{4a} &= T_1\left(f_2\left({R_{11}}^2 + 2 f_4 + {R_{22}}^2\right) + \left({R_{22}}^2 + f_2\right)^2\right), \\ b_{4b} &= -T_2\left(f_5 + f_6\right)\left({R_{11}}^2 + 2 f_2 + {R_{22}}^2\right), \\ b_{div} &= B_{udL}\left(R_{12}{T_2}^2 - R_{21}{T_1}^2 + R_{11}T_1T_2 - R_{22}T_1T_2\right) \end{aligned} \tag{A.7}$$

Automatic Design of Robust Controllers for Grid-Tied Inverters based on PSO and Kharitonov's Theorem ⋆

Caio R. D. Osório[*,**], **Lucas C. Borin**[*], **Gustavo G. Koch**[*], **Everson Mattos**[*], **Pablo García**[***], **Vinicius F. Montagner**[*]

[*] *Federal University of Santa Maria, RS, Brazil*
[**] *Currently a visiting researcher at the University of Oviedo, Spain.*
[***] *Electrical Engineering Department, University of Oviedo, Spain*
(e-mail: caio.osorio@gmail.com)

Abstract: This paper provides an offline procedure for automatic tuning of robust PI controllers applied to the control of LCL-filtered grid-tied inverters. A particle swarm optimization algorithm is used to tune the control gains based on an objective function, which encompasses frequency and time domain specifications, a limit for the control signal, together with a theoretical assessment of robust stability, by means of Kharitonov's Theorem. Experimental results based on hardware-in-the-loop are provided, confirming that the proposed procedure leads to controls gains that ensure robust stability and suitable grid-injected currents under uncertain grid impedances, complying with the IEEE 1547 Standard and with superior performance when compared to other design alternatives.

Keywords: Grid-tied inverter, LCL filter, Robust control, Kharitonov's theorem, Particle swarm optimization.

1. INTRODUCTION

In the scenario of renewable energy systems, a key element is the current control of grid-tied inverters (GTIs), which allows to regulate the power flow between energy sources and the mains (Teodorescu et al., 2011). Moreover, the grid currents must comply with different requirements, suchs as the limits for harmonic distortion of the IEEE 1547 Standard (IEEE, 2011). Therefore, considering the switched nature of the voltage source inverters, output low-pass filters are usually required to interface with the grid, being the LCL filter topology widely used due to the ability to provide suitable high frequency attenuation with reasonable size of magnetics (Ben Saïd-Romdhane et al., 2017).

A widely used alternative for the current control of GTIs with LCL filters are the grid current feedback with proportional-integral (PI) controllers, implemented in synchronous reference frame (Bao et al., 2013). In this context, one important issue is to deal with the inherent resonance peak of the filter, that must be damped by suitable passive or active strategies in order to achieve a stable operation (Dannehl et al., 2010; Hanif et al., 2014). Combined with the appropriate damping technique, the PI controllers have the advantage of being simple, and designs carried out considering only nominal parameters can ensure good performance under stiff grid conditions and when parametric uncertainties are not significant (Chen et al., 2012). On the other hand, the low frequency gain and the crossover frequency of the system have to be reduced to ensure performance and stability when dealing with uncertain parameters, such as the uncertain grid impedances. Thus, the design becomes more difficult, relying on heuristic choices, which usually demand more time from the control designer in trial and error procedures (Pan et al., 2015).

In this context, metaheuristic algorithms are an alternative for the automatic tune of controllers that must cope with multiple objectives and constraints, specially when the objectives are difficult to be expressed analytically (Deb, 2001; Haupt and Haupt, 2004). Among metaheuristic techniques, one can highlight the particle swarm optimization (PSO), a bio-inspired algorithm with simple computational implementation (Eberhart and Kennedy, 1995). The PSO is based on intelligent swarms of particles, that moves in a search space guided by the minimization of an objective function, without relying on its derivative and with good ability to avoid local minima (Sebtahmadi et al., 2017). The PSO algorithm has been used in the literature to tune PI controllers for GTI applications. For instance, in Althobaiti et al. (2016) and Al-Saedi et al. (2011), online optimizations are used to adapt the control gains, while in Hassan and Abido (2011) and de Oliveira et al. (2016), offline optimizations are used to tune fixed controllers. A common point in these works is not including frequency domain specifications in the objective functions, which are useful criteria, often employed in control design of power converters. In Osório et al. (2019), fixed control gains are tunned by the PSO based on the phase margin and crossover frequency. However, although the results illustrate suitable results against uncertain grid induc-

⋆ This study was financed in part by the Coordenação de Aperfeiçoamento de Pessoal de Nível Superior - Brasil (CAPES/PROEX) - Finance Code 001, INCT-GD, CNPq (465640/2014-1, 160884/2019-5 and 309536/2018-9), CAPES (23038.000776/2017-54), FAPERGS (17/2551-0000517-1), and CAPES-PRINT (88887.465639/2019-00).

tances, the paper does not include a theoretical certificate of robust stability.

In this direction, assuming that the plant is described by a model whose coefficients are not precisely known, but belong to real intervals, the robust stability under uncertain parameters can be theoretically certified by Kharitonov's Theorem (Bhattacharyya and Keel, 1995; Bernstein and Haddad, 1990). In the context of power electronics, for instance, Kharitonov's Theorem is used to assess robust stability against circuit parametric uncertainties in Yang et al. (2015) and Hote et al. (2009). Nevertheless, in these previous works, Kharitonov's Theorem has been applied to define the regions of robust stability employed for choosing the control gains, but the use of this tool during the control tuning stage is still worthy of investigation.

The main contribution of the present work is a procedure for the automatic tunning of robust PI controllers applied to current control of LCL-filtered GTIs. The procedure is executed offine and combines PSO and Kharitonov's Theorem to cope with multiple practical design constraints and robustness against parametric uncertainties. The resulting PI controllers rely on fixed gains that can be easily implemented, avoiding more complex strategies (e.g. adaptive strategies) and also reducing the time demanded from a control engineer during the design stage. As performance criteria, the proposed PSO algorithm encompass time and frequency domain specifications, such as the deviation from reference values for phase margin and crossover frequency and limits for gain margin, overshoot, steady state error and control signal saturation. The robust stability of the closed-loop systems have a theoretical certificate through Kharitonov's Theorem, which is a sufficient condition that can be tested in a fast way during the optimization, by evaluating the stability of only four polynomials. Experimental results based on hardware-in-the-loop are provided, validating the proposed procedure and also to establishing a comparison with the results obtained based on other design alternatives.

2. MODELING AND PROBLEM DESCRIPTION

Consider a three-phase inverter connected to the grid through an LCL filter, as shown in Figure 1, where L_c and L_{g1} are the converter-side and grid-side filter inductances, respectively. The filter parasitic resistances are given by r_c and r_{g1}, C_f is the filter capacitance and R_f is the damping resistance, in series with the capacitor. The grid is modeled with a background voltage v_g, in series with a grid resistance r_{g2} and an uncertain grid impedance L_{g2}, lying in a bounded interval whose limits are known.

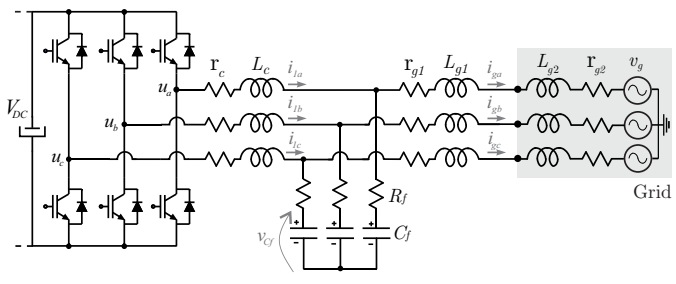

Figure 1. Three-phase grid-tied inverter with LCL filter.

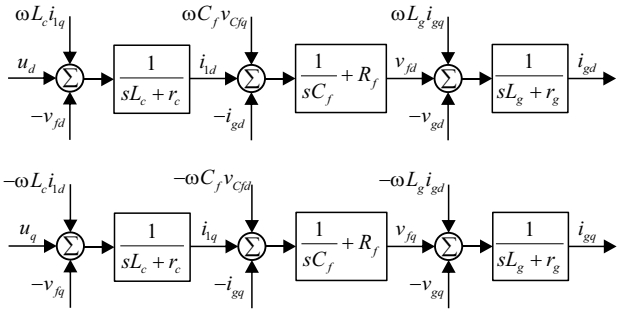

Figure 2. Block diagram of the plant in synchronous reference frame.

In the synchronous reference frame, Figure 2 shows the block diagram of the plant, where $L_g = L_{g1} + L_{g2}$, $r_g = r_{g1} + r_{g2}$ and ω is the grid angular frequency.

Assuming that the three-phase grid voltages are sinusoidal and balanced, they can be neglected at this point (i.e., $v_{gd} = v_{gq} = 0$), being treated as external disturbances (Hanif et al., 2014). Moreover, for the purpose of control design in synchronous reference frame, an usual way to derive the transfer function of the LCL system is to neglect the coupling terms between d-axis and q-axis, also considering them as external disturbance signals, which greatly simplify the modeling (Xuetao et al., 2015).

Considering the previous assumptions, the transfer function from the inverter output voltage $u(s)$ to the grid-injected current $i_g(s)$, valid for both d-axis and q-axis, is given by

$$G(s) = \frac{i_g(s)}{u(s)} = \frac{f_1 s + 1}{g_3(L_g)s^3 + g_2(L_g)s^2 + g_1(L_g)s + g_0} \tag{1}$$

where

$$\begin{aligned} &f_1 = C_f R_f, \\ &g_3(L_g) = C_f L_c L_g, \\ &g_2(L_g) = C_f R_f\,(L_c + L_g) + C_f L_c r_g + C_f L_g r_c, \\ &g_1(L_g) = L_c + L_g + R_f r_g C_f + C_f r_c\,(R_f + r_g), \\ &g_0 = r_g + r_c \end{aligned} \tag{2}$$

Notice that, due to the uncertainty in the grid inductance L_{g2}, the parameter L_g is also uncertain, lying in the interval $[L_{gmin}, L_{gmax}]$. Therefore, g_3, g_2 and g_1 can be written as interval coefficients lying in bounded real intervals, that depend on L_g.

In order to control the grid-injected currents, a single-loop grid current feedback control is employed here, for both d-axis and q-axis, with a PI controller given by

$$C(s) = \frac{K_P s + K_I}{s} \tag{3}$$

with fixed coefficients, defined by the vector

$$c = [K_I \quad K_P] \tag{4}$$

The block diagram of the closed-loop system is shown in Figure 3, for the d-axis. To mitigate the effect of the grid voltage, this disturbance is feedforward in the control action. Also, a compensation decoupling term is included, given by $dec = \omega(L_c + L_g)i_{gq}$, aiming to mitigate the dynamic effect of the inherent coupling between the axes. An analogous block diagram is valid for the q-axis.

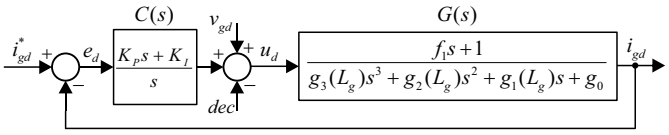

Figure 3. Block diagram of the closed-loop system for the d-axis grid current control

It should be noted that the single-loop control method for LCL filters is very susceptible to the resonance peak, being performance and stability highly dependent on the damping of the system. Moreover, the stability and performance are also highly dependent on parameter uncertainties, since the low frequency gain and control bandwidth must be reduced to ensure stability of the system in the entire range of the parameters (Pan et al., 2015; Sivadas and Vasudevan, 2018).

In this context, the control problem to be solved for this case study is to synthesize, with an offline and automatic procedure, fixed gains for the PI controller in (3), that ensure stability and suitable dynamic performance for the entire range of L_g.

3. ASSESSMENT OF ROBUST STABILITY AND PERFORMANCE

In order to develop an automatic procedure for the tunning of the control gains in (4), it is important to assess the robust stability and performance of the closed-loop system depicted in Figure 3 in a computationally efficient way.

3.1 Robust stability based on Kharitonov's Theorem

Considering a closed-loop system based on a plant subject to uncertain parameters and a controller with fixed control gains, the theoretical robust stability can be easily certified by means of Kharitonov's Theorem.

Given the plant (1), with interval coefficients, and the PI controller (3), the characteristic polynomial of the closed-loop system can be written in the interval form as

$$D(s) = d_0 + d_1 s + d_2 s^2 + d_3 s^3 + d_4 s^4 \tag{5}$$

with coefficients lying in bounded real intervals

$$d_\ell \in \left[{d_\ell}^-, {d_\ell}^+ \right] \quad , \quad \ell = 0, \cdots, 4 \tag{6}$$

where

$$\begin{array}{l} {d_0}^- = {d_0}^+ = K_I; \\ {d_1}^- = {d_1}^+ = g_0 + f_1 K_I + K_P; , \\ {d_2}^- = g_1(L_{gmin}) + f_1 K_P, \quad {d_2}^+ = g_1(L_{gmax}) + f_1 K_P; \\ {d_3}^- = g_2(L_{gmin}), \quad {d_3}^+ = g_2(L_{gmax}); \\ {d_4}^- = g_3(L_{gmin}), \quad {d_4}^+ = g_2(L_{gmax}). \end{array} \tag{7}$$

According to Kharitonov's Theorem, one has that if the four polynomials (Bhattacharyya and Keel, 1995)

$$\begin{array}{l} K_1(s) = {d_o}^- + {d_1}^- s + {d_2}^+ s^2 + {d_3}^+ s^3 + {d_4}^- s^4 \\ K_2(s) = {d_o}^- + {d_1}^+ s + {d_2}^+ s^2 + {d_3}^- s^3 + {d_4}^- s^4 \\ K_3(s) = {d_o}^+ + {d_1}^- s + {d_2}^- s^2 + {d_3}^+ s^3 + {d_4}^+ s^4 \\ K_4(s) = {d_o}^+ + {d_1}^+ s + {d_2}^- s^2 + {d_3}^- s^3 + {d_4}^+ s^4 \end{array} \tag{8}$$

are Hurwitz, then $D(s)$ in (5) is Hurwitz and thus, the closed-loop system with control gains K_P and K_I is stable for all values of the $L_g \in [L_{gmin}, L_{gmax}]$.

Therefore, if (8) is satisfied in the scenario specified above, the uncertain closed-loop system will be called from now on, in this paper, as *KT stable*, i.e., stable based on Kharitonov's Theorem.

It should be mentioned that when the coefficients of $D(s)$ in (5) are not independent, i.e., the uncertain parameter L_g appears in more than one coefficient of the transfer function (1) at the same time, then Kharitonov's Theorem tested as in (8) is a sufficient condition for robust stability of the closed-loop system with a given controller (3) (Bhattacharyya and Keel, 1995). Nevertheless, due to its computational simplicity, it is still worth to be used for a fast evaluation of stability.

3.2 Performance criteria based on polytopic representation

In classical control design procedures for power converters, it is very common to specify performance in terms of frequency domain criteria, such as crossover frequency (ω_{co}), phase margin (PM) and gain margin (GM) (Buso and Mattavelli, 2006; Teodorescu et al., 2011). Moreover, it is also desirable to shape the closed-loop system step response based on time domain performance constraints, such as overshoot (OV) and steady state error (e_{ss}). A good trade-off among all these specifications can be a challenge, becoming more difficult when uncertain parameters and control saturation (i.e., a limit for the amplitude of the control signal u) must be taken into account in the design stage.

Given a controller with fixed gains, one way to estimate the above performance measures for plants affected by uncertain parameters is from a polytopic representation of the system (Karimi et al., 2007).

Considering the plant (1) and the controller (3), the closed-loop system must be designed to ensure suitable performance against the uncertain parameter L_g. By taking into account the extreme values of this parameter, from (1), the resulting polytopic model is limited to 2 vertices, i.e., considering L_{gmin} and L_{gmax}. Therefore, the measures of PM, ω_{co}, GM, OV, e_{ss} and the maximum value of u can be carried out evaluating the time and frequency domain responses at these vertices.

Notice that even though the worst case values of the above measures may not be captured by only evaluating the vertices of the polytope, the proposed procedure becomes appealing from the computational point of view, leading to effective results, as will be shown in the sequence.

4. PROPOSED CONTROL DESIGN PROCEDURE

In this Section, it is proposed an offline automatic procedure to find the control gains of the PI controller in (4), such that: a) the closed-loop uncertain system (1) with controller (3) is *KT stable*; b) an objective function including performance specifications in terms of the time and frequency domain criteria is optimized in the vertices of the polytopic model.

To accomplish that, consider the optimization problem

$$c^\star = \arg \min_{c \in \mathcal{C}} \ f(c) \tag{9}$$

where $c^\star$ is the best controller associated with the vector c, given in (4), which minimizes the objective function $f(c)$ in a given search space $\mathcal{C}$.

The definition of the objective function, the search space for the gains and the optimization algorithm is given in the sequence.

4.1 Objective function

To measure the quality of the system performance with a given controller candidate c, in (4), the objective function proposed here is given by

$$f(c) \;=\; \alpha(c)\;\beta(c)\;\gamma(c) \tag{10}$$

returning a real positive scalar computed based on three terms, $\alpha(c)$, $\beta(c)$ and $\gamma(c)$.

First, assume a reference value PM^*, for the phase margin, and ${\omega_{co}}^*$, for the crossover frequency. Then, the term $\alpha(c)$ is given by

$$\alpha(c) = \max_{j=1,2}\left(\left|\frac{\mathrm{PM}^* - \mathrm{PM}_j(c)}{\mathrm{PM}^*}\right| + \left|\frac{{\omega_{co}}^* - \omega_{coj}(c)}{{\omega_{co}}^*}\right|\right) \tag{11}$$

and measures the worst case deviation of the phase margin and crossover frequency to the respective references. The values of $\mathrm{PM}_j(c)$ and $\omega_{coj}(c)$ are obtained from the transfer function

$$T_j(s) = C(s)G_j(s) \tag{12}$$

which is evaluated for each vertex of the polytopic model, represented by the index j, with a given controller candidate $C(s)$, whose coefficients are given by the vector c. These values can be easily obtained by means of specialized functions, such as the function *margin*, from MATLAB.

To improve the time and frequency responses, a term $\beta(c)$ is taken into account, including additional constraints to the objective function, such that

$$\beta(c) = \begin{cases} 1, & \begin{array}{l}\text{if } \mathrm{GM}_j(c) \geq \underline{\mathrm{GM}} \text{ and } \mathrm{OV}_j(c) \leq \overline{\mathrm{OV}} \\ \text{and } |e_{ssj}(c)| \leq \overline{e_{ss}} \text{ and } |u_j(c)| \leq \overline{u} \\ \text{for } j = 1, 2\end{array} \\ 10^6, & \text{otherwise} \end{cases} \tag{13}$$

The term $\beta(c)$ returns an unitary value if all the conditions in (13) are satisfied, i.e., if the controller candidate c ensures, for each vertex, compliance with prescribed lower bound $\underline{\mathrm{GM}}$ and upper bounds $\overline{\mathrm{OV}}$, $\overline{e_{ss}}$ and $\overline{u}$. Otherwise, $\beta(c)$ returns the value 10^6, in order to penalize the objective function for this controller candidate. The indices in (13) can be easily computed, for instance, by means of the functions *margin* and *step*, from MATLAB.

The third term of the proposed objective function, $\gamma(c)$, is related with the robust stability ensured by means of Kharitonov's Theorem, and is given by

$$\gamma(c) = \begin{cases} 1, & \text{if closed-loop system is } \textit{KT stable} \\ 10^6, & \text{otherwise} \end{cases} \tag{14}$$

Note that a positive evaluation of Kharitonov's Theorem is a theoretical guarantee of robust stability for the closed-loop system under uncertain parameter $L_g \in [L_{gmin}, L_{gmax}]$.

It is worth to mention that different objective functions could be defined to guide the control design task. The specifications in (10) were chosen here because, besides considering traditional performance constrains in power electronics (e.g., PM, GM, ω_{co}), they include as a contribution, the robust stability assessment (i.e. *KT stability*) and actuator saturation evaluation in the control design stage.

4.2 Search space

From the definition of the controller coefficients in (4), the space for searching the control gains is given by

$$\mathcal{C} = \begin{cases} (K_I, K_P) \in \mathcal{R}^2 \\ {K_I}^- \leq K_I \leq {K_I}^+, \;\; {K_P}^- \leq K_P \leq {K_P}^+ \end{cases} \tag{15}$$

and is defined here based on the positivity of the coefficients of polynomial (5), for all possible combinations of $L_g \in [L_{gmin}, L_{gmax}]$. This choice is based on the well-known necessary condition for Hurwitz stability. Although it tends to produce a large search space, the advantage is that this space can be systematically obtained in a fast way from a set of linear inequalities, by solving a linear programming problem, and then, including the resulting region in a hyperrectangle, as describe in (15).

Therefore, from (5)–(7), the inequalities used to define the search space are given by

$$\begin{array}{l} K_I > 0 \\ C_f R_f K_P > -(L_c + L_{gmin} + R_f r_g C_f + C_f r_c\,(R_f + r_g)) \\ C_f R_f K_I + K_P > -(r_g + r_c) \end{array} \tag{16}$$

where the second inequality is evaluated for L_{gmin} since this condition leads to the more restrictive search space.

It is worth to notice that belonging to this search space is a necessary (but no sufficient) condition to the system stability over the entire range of parameters. More accurate search spaces could be obtained applying, for instance, the complete Routh-Hurwitz criterion, but at the price of more time-consuming and complex calculations to define the search space.

Since $\mathcal{C}$ can be a large search space, exhaustive grid techniques are usually unviable for a high resolution discretization. In this scenario, metaheuristics such as the PSO algorithm has proven to be useful.

4.3 Particle swarm optimization

In the context of the PSO applied to the design problem in this paper, each possible control gain vector c, in (4), can be associated with a particle i, whose position in the search space is given by

$$s_i = [K_{Ii}, K_{Pi}], \quad i = 1, \cdots, N \tag{17}$$

where N is the number of particles in the swarm.

The particles are randomly initialized on the search space $\mathcal{C}$. In a given epoch k, the objective function (10) is evaluated for each particle, based on its position s_i^k. The swarm of particles move in the search space from one epoch k to the next epoch $k+1$, until reaching the stop criterion. Therefore, each particle moves from the position s_i^k to the next position s_i^{k+1}, with a velocity v_i^{k+1}, according to the equations

$$s_i^{k+1} \;=\; s_i^k \;+\; v_i^{k+1} \tag{18}$$

$$v_i^{k+1} = \lambda v_i^k + \phi_1\, r_1(P_{i.best} - s_i^k) + \phi_2\, r_2(G_{best} - s_i^k) \quad (19)$$

The velocity of a given particle is influenced by the best position that it got ($P_{i.best}$), and also by the best position among all particles of the swarm (G_{best}). ϕ_1 is the cognitive coefficient, ϕ_2 is the social coefficient, λ is the inertia factor and r_1 and r_2 are random values between $[0, 1]$.

Regarding the configuration of the PSO algorithm, the number of particles N and the coefficients ϕ_1 and ϕ_2 are set in order to ensure convergence of the objective function with viable computational effort. The algorithm stop criterion can be set as reaching a maximum number of epochs M, or on stalling of the objective function. For instance, using MATLAB, this algorithm can be easily executed using the *particleswarm* function, which present default values for these configurations.

4.4 Summary of the proposed procedure

The proposed design procedure can be summarized by the following steps:

I. Define the system nominal and interval parameters and obtain the plant model (1);
II. Define the control structure and the controller coefficients, as shown in (3) and (4), for the PI controller;
III. Choose the frequency and time domain specifications of the objective function, in (11) and (13);
IV. Based on the characteristic polynomial of the closed-loop system, in (5), determine the search space (15);
V. Set the PSO configurations and run the algorithm.

It is worth to recall that, in each iteration of the PSO, each particle (candidate controller) is evaluated based on the objective function (10), including the assessment of robust stability using Kharitonov's Theorem.

After the execution, if the algorithm converges to a controller $c^\star$ (best particle of the swarm), for which $\beta(c^\star) = 1$ and $\gamma(c^\star) = 1$, all the constraints in (13) are satisfied and the closed-loop robust stability is successfully accessed by Kharitonov's Theorem. Thus, the procedure ends, providing $c^\star$ as a viable robust controller.

If the algorithm converges to a *KT stable* controller, but it is unable to satisfy the constraints in (13), one option is to execute the procedure again, redefining the PSO parameters (for intance, increasing the number of particles and epochs). Alternatively, if necessary, the objective function specifications can be relaxed to obtain a viable controller.

5. DESIGN EXAMPLE

Following the first step of the proposed procedure, consider the parameters of the LCL-filtered grid-tied inverter given in Table 1. The parasitic resistances are neglected, and the grid inductance is an uncertain parameter lying in a bounded interval.

For the second step, the control structure is defined as the one given in Figure 3, with the PI controller.

The third step in the proposed procedure is to choose the objective function specifications. Thus, the reference values for system performance and stability margins are specified as

Table 1. System parameters

System description	
Switching frequency f_{sw}	10020 Hz
Sampling frequency f_s	20040 Hz
DC-link V_{dc}	400 V
Grid voltage V_g	220 Vrms, 60 Hz
Converter inductance L_c	1 mH
Grid-side inductance L_{g1}	0.3 mH
Filter capacitor C_f	62 μF
Grid inductance $[L_{g2min}, L_{g2max}]$	[0.1 1.5] mH
Grid resistance r_g	0.1 Ω
Damping resistance R_f	1 Ω

$$\underline{\omega_{co}}^* = 600 \text{ rad/s} \quad \text{PM}^* = 60^\circ \quad \underline{\text{GM}} = 5\ (14\ dB)$$
$$\overline{\text{OV}} = 10\% \quad \overline{e_{ss}} = 0\% \quad \overline{u} = 1 \quad (20)$$

Regarding the step IV, the limits of the search space are defined based on (15) and (16). For simplicity, a rectangular region with $K_P > 0$ and $K_I > 0$ is considered, and the upper bounds are set as 10^4, in order to have a large region for searching both control gains.

For the last step, the PSO is configured with parameters

$$\text{N} = 200 \text{ particles, M} = 50 \text{ epochs, } \phi_1 = 0.5,\ \phi_2 = 0.5 \quad (21)$$

and the algorithm is executed.

To illustrate the success rate of the results, the algorithm was executed 20 times, having always converged in about 3 minutes to a viable controller with low deviation of the gains among the executions. For a typical execution, the evolution of the best value of $f(c)$ in each epoch (called fitness) is depicted in Figure 4(a), and the control gains are given by

$$c^\star = [K_I \ K_P] = [102.13418 \ \ 0.95822] \quad (22)$$

The closed-loop system in Figure 3 was simulated with the control gains in (22). The step responses of the closed-loop system for the extreme values of grid inductances are shown in Figure 4(b), where the maximum overshoot is $\text{OV}_{max} = 8.88\%$ and there is no error in steady state.

The frequency responses of the open-loop transfer function $T(s) = C(s)G(s)$ is shown in Figure 5, for L_{gmin} and L_{gmax}, which confirm system stability for the entire range of parameters. The minimum values of the stability margins and crossover frequency were achieved with L_{gmax}, for which $\text{GM}_{min} = 14.1\ dB$, $\text{PM}_{min} = 79.1^\circ$, $f_{comin} = 56.8$ Hz (≈ 357 rad/s). From the results shown in Figures 4 and 5, it is possible to confirm that all constraints in (20) were satisfied.

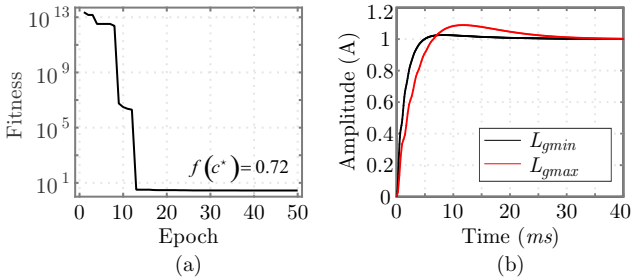

Figure 4. Results for a typical execution: (a) Fitness curve; (b) Step responses with gains (22).

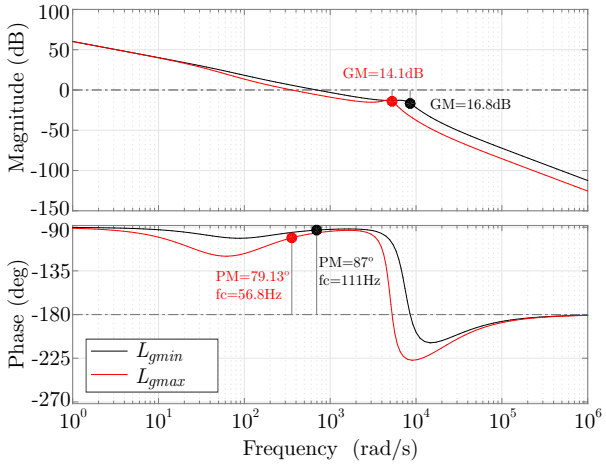

Figure 5. Bode diagrams with gains (22), from i_{ref} to i_g.

5.1 Experimental Results based on HIL

Real-time tests based on hardware-in-the-loop (HIL) are presented to validate the control gains designed with the proposed procedure. The LCL-filtered GTI depicted in Figure 1 was emulated with parameters in Table 1, using a Typhoon HIL, model 402.

For the digital implementation, consider the discretization of the PI controller (22) using the Tustin method, with the sampling frequency given in Table 1. The DSP TMS32F28335, from Texas Instruments, is used to implement the controllers, assuming the same gains for both d and q axes, including the feedforward of the grid voltage and also the decoupling terms, as shown in Section 2. The angle for the Park transform (i.e., to obtain the signals in dq coordinates) is obtained using a Kalman Filter algorithm, ensuring that the three-phase grid currents are synchronized with the voltages at the point of common coupling (Cardoso et al., 2008). To drive the inverter switches, a space vector modulation is employed.

Figure 6 shows the grid current responses, in d-axis and q-axis, for sudden variations in the grid current references, considering the extremes of the uncertain parameter L_g. The first variation represents the start-up of the system, injecting active power into the grid, while the second variation represents a transient from active to reactive power. It is possible to verify that, with the PSO-based PI controller, the closed-loop system is able to track the references respecting the performance constraints established in the design and also with suitable settling times, for both grid conditions. The transient responses for L_{gmax} are slower than the responses for L_{gmin}, which is expected due to the need of ensuring robustness over the entire range of parameters with a simple fixed gain controller.

In order to establish a comparison between the proposed procedure and an well-known tuning technique, Figure 6 also shows the responses with a PI controller designed using the *pidtune* function, from MATLAB. In this case, the controller was designed for L_{gmax}, and considering the same specifications used for the PSO: $\omega_{co}{}^{*} = 600$ rad/s and PM$^{*} = 60°$. It is possible to verify superior performance of the closed-loop system with the PI controller designed based on the proposed procedure. A more detailed

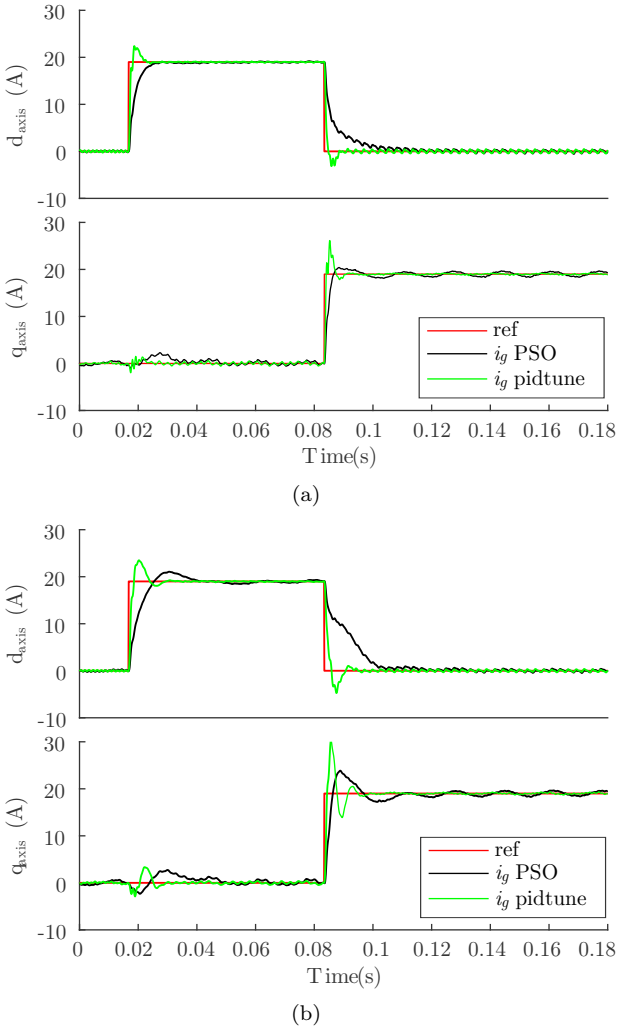

Figure 6. Step responses with the PSO-based and the *pidtune* PI controllers, for: (a) L_{gmin}; (b) L_{gmax}.

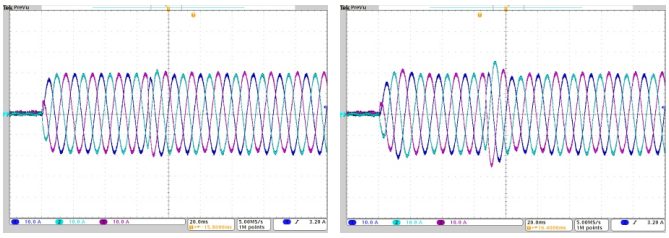

(a) (b)

Figure 7. Transient responses of the three-phase grid currents for the system operating with the PSO-based PI controller and: (a) $L_g = L_{gmin}$; (b) $L_g = L_{gmax}$

performance comparison will be presented in Table 2, in the next section.

For the system operating with the PSO-based controller, the three-phase grid currents with respect to the transient responses presented in Figure 6(a) and (b) are shown in Figure 7(a) and Figure 7(a), respectively. From these results, it is possible to confirm robust stability and suitable transient performances for both extreme values of the grid inductances.

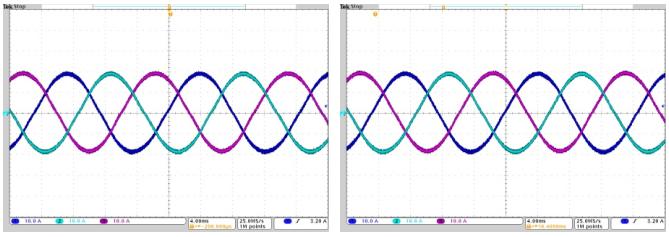

(a) (b)

Figure 8. Three-phase grid currents in steady-state for the system operating with the PSO-based PI controller and: (a) $L_g = L_{gmin}$; (b) $L_g = L_{gmax}$.

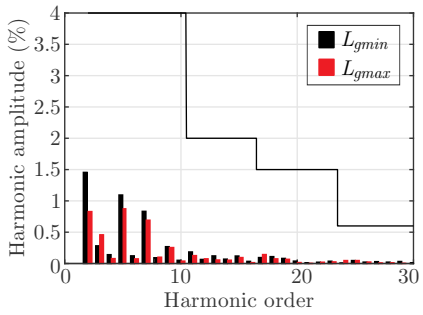

Figure 9. Steady-state responses: current harmonic spectrum and limits from IEEE 1547.

The grid currents in steady-state are highlighted in Figure 8(a), for $L_g = L_{gmin}$, and in Figure 8(b), for $L_g = L_{gmax}$. From these waveforms, Figure 9 shows that the harmonic spectra of the grid currents comply with the requirements of the IEEE 1547 Standard, for both extreme values of L_g. Moreover, the total harmonic distortion (THD) is equal to 2.13%, for L_{gmin}, and 1.59%, for L_{gmax}, also complying with this standard (THD $\leq$ 5%).

6. COMPARATIVE ANALYSIS

For a comparative analysis, Table 2 shows performance criteria obtained with controllers designed using the proposed procedure and two other control tunning strategies. The measures given in the Table 2 are the worst case values for each design specification, obtained based on simulations for the vertices of the polytopic model.

First, consider the controller designed using the *pidtune* function, from MATLAB, with experimental results already shown in Figure 6. The measurement of the performance criteria with this controller is better detailed in the second column of Table 2, from which it is possible to verify that it led to acceptable closed-loop responses. On the other hand, in comparison with the proposed PSO-based controller, the performance are inferior in terms of gain margin and overshoot. Moreover, the *pidtune* controllers do not have a theoretical certificate of robust stability under parametric uncertainties and also may lead to control saturation.

In order to provide a comparison between the PSO and a different optimization tool, consider the genetic algorithms (GA), which are a well established metaheuristic that could have been used in the proposed procedure (Haupt and Haupt, 2004). In this sense, a GA is configured here using the same objective function proposed in (10) and with parameters similar to the ones used for the PSO (e.g. same number of particles for PSO and chromosomes for GA, epochs for PSO and generations for GA). Columns 1 and 3 of Table 2 show that both PSO and GA lead to similar results in terms of phase margin, crossover frequency, gain margin and overshoot. On the other hand, a statistical analysis performed when repeating 20 times the execution of both algorithms shows that, in comparison to the GA, the PSO has the advantage of converging, in average, in half the time. Moreover the PSO executions present a higher success rate and a lower dispersion of the solutions. This analysis is summarized in Table 3, confirming that the PSO is a suitable optimization algorithm for the proposed procedure.

To obtain the statistics in Table 3, the success rate was defined by the ratio between the number of successful executions and the total number of executions, where a successful execution is when the algorithm converged to a controller $c^\star$ that has $\beta(c^\star) = 1$ and $\gamma(c^\star) = 1$. The dispersion was defined as the standard deviation of the value $f(c^\star)$ divided by its average value.

Table 2. Design comparisons

	PSO	Pidtune	GA
PM (deg)	79.13	60.1	79.24
ω_c (rad/s)	356.88	955.04	354.75
GM (dB)	14.1	6.34	14
OV (%)	8.88	27.0	8.75
Saturation	No	Yes	No
KT stable	Yes	No	Yes
K_P	0.958	2.190	0.952
K_I	102.1	1300	99.99

Table 3. Statistics Comparison between GA and PSO Algorithms

	PSO	**GA**
Success rate	100%	60%
Dispersion	0.824%	4.52%

7. CONCLUSION

This paper proposed a procedure for the automatic tunning of robust PI controllers applied to LCL-filtered GTIs. A PSO algorithm is employed to optimize an objective function for the vertices of a polytope, taking into account important frequency and time-domains criteria. During the optimization, the PSO is capable of finding PI control gains which ensure, for the entire domain of grid impedances, suitable performances and the robust stability certified by Kharitonov's Theorem. This theorem is used here within the optimization procedure, and not in an a priori fashion to determine the region for the search of the control gains. Experimental results based on HIL confirm that the proposed procedure leads to viable controllers, ensuring robust stability, suitable dynamic performance and compliance with the IEEE 1547 Standard. Therefore, the proposed procedure can be seen as an alternative for automatic tunning of controllers that must cope with multiple specifications, avoiding time-consuming design stages, specially considering robust stability against uncertain parameters.

REFERENCES

Al-Saedi, W., Lachowicz, S.W., and Habibi, D. (2011). An optimal current control strategy for a three-phase grid-connected photovoltaic system using particle swarm optimization. In *2011 IEEE Power Engineering and Automation Conference*, volume 1, 286–290.

Althobaiti, A., Armstrong, M., and Elgendy, M.A. (2016). Control parameters optimization of a three-phase grid-connected inverter using particle swarm optimisation. In *8th IET International Conference on Power Electronics, Machines and Drives (PEMD 2016)*, 1–6.

Bao, X., Zhuo, F., Tian, Y., and Tan, P. (2013). Simplified feedback linearization control of three-phase photovoltaic inverter with an LCL filter. *IEEE Transactions on Power Electronics*, 28(6), 2739–2752.

Ben Saïd-Romdhane, M., Naouar, M.W., Slama-Belkhodja, I., and Monmasson, E. (2017). Robust active damping methods for LCL filter-based grid-connected converters. *IEEE Transactions on Power Electronics*, 32(9), 6739–6750.

Bernstein, D.S. and Haddad, W.M. (1990). Robust controller synthesis using kharitonov's theorem. In *29th IEEE Conference on Decision and Control*, 1222–1223.

Bhattacharyya, S.P. and Keel, L.H. (1995). Robust control: the parametric approach. In *Advances in Control Education 1994*, 49–52. Elsevier.

Buso, S. and Mattavelli, P. (2006). *Digital Control in Power Electronics*. Morgan & Claypool Publishers.

Cardoso, R., de Camargo, R.F., Pinheiro, H., and Gründling, H.A. (2008). Kalman filter based synchronisation methods. *IET Generation, Transmission Distribution*, 2(4), 542–555.

Chen, X., Gong, C.Y., Wang, H.Z., and Cheng, L. (2012). Stability analysis of LCL-type grid-connected inverter in weak grid systems. In *2012 International Conference on Renewable Energy Research and Applications (ICRERA)*, 1–6.

Dannehl, J., Fuchs, F., Hansen, S., and Thøgersen, P. (2010). Investigation of active damping approaches for PI-based current control of grid-connected pulse width modulation converters with LCL filters. *IEEE Transactions on Industry Applications*, 46(4), 1509 – 1517.

Oliveira, F.M., Oliveira da Silva, S.A., Durand, F.R., Sampaio, L.P., Bacon, V.D., and Campanhol, L.B.G. (2016). Grid-tied photovoltaic system based on pso mppt technique with active power line conditioning. *IET Power Electronics*, 9(6), 1180–1191.

Deb, K. (2001). *Multi-objective optimization using evolutionary algorithms*, volume 16. John Wiley & Sons.

Eberhart, R. and Kennedy, J. (1995). A new optimizer using particle swarm theory. In *In Proceedings of the Sixth International Symposium on Micro Machine and Human Science.*, 39–43.

Hanif, M., Khadkikar, V., Xiao, W., and Kirtley, J.L. (2014). Two degrees of freedom active damping technique for LCL filter-based grid connected pv systems. *IEEE Transactions on Industrial Electronics*, 61(6), 2795–2803.

Hassan, M.A. and Abido, M.A. (2011). Optimal design of microgrids in autonomous and grid-connected modes using particle swarm optimization. *IEEE Transactions on Power Electronics*, 26(3), 755–769.

Haupt, R. and Haupt, S. (2004). *Practical Genetic Algorithms*. Wiley-Interscience publication. John Wiley.

Hote, Y.V., Choudhury, D.R., and Gupta, J. (2009). Robust stability analysis of the PWM push-pull DC–DC converter. *IEEE transactions on power electronics*, 24(10), 2353–2356.

IEEE (2011). IEEE:1547 standard for interconnecting distributed resources with electric power systems.

Karimi, A., Khatibi, H., and Longchamp, R. (2007). Robust control of polytopic systems by convex optimization. *Automatica*, 43(8), 1395–1402.

Osório, C.R.D., Borin, L.C., Koch, G.G., and Montagner, V.F. (2019). Optimization of robust pi controllers for grid-tied inverters. In *2019 IEEE 15th Brazilian Power Electronics Conference and 5th IEEE Southern Power Electronics Conference (COBEP/SPEC)*, 1–6.

Pan, D., Ruan, X., Bao, C., Li, W., and Wang, X. (2015). Optimized controller design for LCL-type grid-connected inverter to achieve high robustness against grid-impedance variation. *IEEE Transactions on Industrial Electronics*, 62(3), 1537–1547.

Sebtahmadi, S.S., Azad, H.B., Kaboli, S.H.A., Islam, M.D., and Mekhilef, S. (2017). A PSO–DQ current control scheme for performance enhancement of Z–source matrix converter to drive IM fed by abnormal voltage. *IEEE Transactions on Power Electronics*, 33(2), 1666–1681.

Sivadas, D. and Vasudevan, K. (2018). Stability analysis of three-loop control for three-phase voltage source inverter interfaced to the grid based on state variable estimation. *IEEE Transactions on Industry Applications*, 54(6), 6508–6518.

Teodorescu, R., Liserre, M., and Rodríguez, P. (2011). *Grid Converters for Photovoltaic and Wind Power Systems*. Wiley - IEEE. John Wiley & Sons.

Xuetao, P., Tiankai, Y., Keqing, Q., Jinbin, Z., Wenqi, L., and Xuhui, C. (2015). Analysis and evaluation of the decoupling control strategies for the design of grid-connected inverter with LCL filter. In *International Conference on Renewable Power Generation (RPG 2015)*, 1–6.

Yang, X., Yuan, Y., Long, Z., Goncalves, J., and Palmer, P.R. (2015). Robust stability analysis of active voltage control for high-power IGBT switching by kharitonov's theorem. *IEEE Transactions on Power Electronics*, 31(3), 2584–2595.

IEEE CPE-POWERENG
Setúbal 2020

CERTIFICATE

I hereby certify that **Caio Osório** attended the 14th International Conference on Compatibility, Power Electronics and Power Engineering (IEEE CPE-POWERENG 2020), hosted from Portugal, on July 8-10, 2020, and presented the paper "***Robust Control of Grid-Tied Inverters using Particle Swarm Optimization and Linear Matrix Inequalities***".

Prof. Dr. João Martins and Prof. Dr. Vitor Pires
(IEEE CPE-POWERENG 2020 Conference Chairmans)

UNINOVA FCT FACULDADE DE CIÊNCIAS E TECNOLOGIA UNIVERSIDADE NOVA DE LISBOA UNIVERSIDADE NOVA DE LISBOA IEEE ICS IPS Instituto Politécnico de Setúbal Escola Superior de Tecnologia de Setúbal

July 8-10, 2020, Setúbal - Portugal

ANEXO (4) - Artigo apresentado no 14th International Conference on Compatibility, Power Electronics and Power Engineering

Robust Control of Grid-Tied Inverters using Particle Swarm Optimization and Linear Matrix Inequalities

Lucas C. Borin, Iury Cleveston, Gustavo G. Koch, Caio R. D. Osório, Everson Mattos, and Vinícius F. Montagner
Power Electronics and Control Research Group – Federal University of Santa Maria
Santa Maria, RS, Brazil
Email: lukascielo@gmail.com

***Abstract*—This paper provides a new design procedure for robust current controllers applied to LCL-filtered grid-tied inverters suitable for the integration of renewable energy sources. The design takes into account the digital implementation delay, multiple resonant controllers and operation under uncertain grid impedance. The procedure is based on the optimization of an objective function that allows to get a good trade-off between the settling of transient responses and rejection of disturbances. A particle swarm algorithm is used to find the optimal control gains and, differently from other works, here the robust stability of the closed-loop system under uncertain parameters is theoretically certified by means of linear matrix inequalities. Experimental results are shown, confirming that the closed-loop system with gains obtained by the proposed procedure presents a good trade-off between robustness and performance, with suitable transients and grid currents with low harmonic content, complying with requirements from IEEE 1547 Standard, becoming a useful robust control design alternative for power converters in the distributed generation scenario.**

***Index Terms*—Grid-tied inverters, Linear matrix inequalities, Particle swarm optimization, Robust control, State feedback.**

I. Introduction

The population growth and the technological development lead to a continuous increase in the consumption of electrical energy. In order to cope with this demand in a sustainable way, renewable energy sources have become an important alternative [1], [2]. In this context, grid-tied inverters (GTIs) play a major role to interface renewable energy sources and the power grid, allowing operation with voltage, frequency and currents complying with stringent standards [3]–[5]. The control of such converters becomes more challenging when dealing with disturbances and uncertain grid impedances at the point of common coupling, which is a typical issue in the scenario of distributed generation and microgrids [6], [7].

One of the key features of GTIs is the control of the grid-injected currents, which allows to regulate the power flow between the primary source and the grid. Several current control strategies have been employed as, for instance, the proportional-integral in synchronous reference frame, proportional resonant in stationary reference frame and also state feedback [8]–[12]. In the case of GTIs with output LCL filters, there is a resonance peak that must be properly attenuated to avoid performance degradation or even instability, being active damping strategies preferred over the passive to avoid additional power losses. The design of active damping strategies becomes more difficult under grid uncertain parameters, motivating the investigation of better trade-offs between performance and robustness. In this way, metaheuristics can be an important alternative to search spaces in order to find the control gains in an optimal way, allowing to take into account practical performance indices, that can be measured even by means of simulations or based on experimental data. However, metaheuristics have not been extensively investigated for control tuning of power converters [13].

Among the metaheuristics, it is worth to highlight the particle swarm optimization (PSO), that can optimize complex functions, with simple implementation and fast execution when compared to other techniques [13], [14]. PSO has already been applied to power converters control design in [15]–[19]. A common point in these works is that robustness against uncertain parameters is not taken into account in the design stage. Moreover, since the calculations in the PSO are performed only for some parameter conditions, it may not be sufficient to ensure robust stability for the entire domain of uncertainties (which has infinite points). On the other hand, one way to represent systems subject to uncertain parameters is by means of polytopic models, from which, given a control gain, linear matrix inequalities (LMIs) can be applied to provide a theoretical certificate of stability for the entire domain of uncertainties, based on a finite number of evaluations. LMIs are recognized as a very efficient tool, being solved by specialized programs in a fast way (solution in polynomial time) [20].

The main motivation for the present work is to provide a design procedure that combines PSO and LMIs, leading to control gains that ensure suitable grid currents even under disturbances, parameter uncertainties and delay from digital control. The proposed procedure is able to find state feedback control gains in a given hyper-rectangle, thanks to the PSO, and also can certify the robust stability of the closed-loop system under uncertain grid impedance, thanks to the LMIs. The optimization which guides the control design is based on a novel objective function, which takes into account a limit for the closed-loop poles and also a limit for the transmission of disturbances from the control input to the system output. Experimental results are presented and confirm the effectiveness of the proposed procedure for grid-current control.

978-1-7281-4218-0/20/$31.00 ©2020 IEEE

II. State Space Model with Uncertainties

A three-phase inverter connected to the grid by means of an LCL filter is shown in Figure 1. The grid is assumed as predominately inductive, and the equivalent grid inductance at the point of common coupling (PCC) is given by the uncertain parameter L_{gr}.

From the inverter output voltages, considering a balanced system and that there is no path for the current $'0'$, a state space model of the plant in $\alpha\beta 0$ stationary reference frame can be written as (see, for instance, [21] for details)

$$\begin{bmatrix} \dot{x}_\alpha \\ \dot{x}_\beta \end{bmatrix} = \begin{bmatrix} A(L_g) & 0 \\ 0 & A(L_g) \end{bmatrix} \begin{bmatrix} x_\alpha \\ x_\beta \end{bmatrix} + \begin{bmatrix} B_u & 0 \\ 0 & B_u \end{bmatrix} \begin{bmatrix} u_\alpha \\ u_\beta \end{bmatrix} + \begin{bmatrix} B_w(L_g) & 0 \\ 0 & B_w(L_g) \end{bmatrix} \begin{bmatrix} v_{g\alpha} \\ v_{g\beta} \end{bmatrix} \tag{1}$$

where x_α and x_β are state vectors, u_α and u_β are control inputs, $v_{g\alpha}$ and $v_{g\beta}$ are disturbance inputs, and the uncertain parameter L_g is given by

$$L_g = L_{c2} + L_{gr} \tag{2}$$

due to the uncertainty on L_{gr}.

Notice that (1) represents two single-phase decoupled systems. For instance, for axis α, this model is given by

$$\dot{x}_\alpha = A(L_g)x_\alpha + B_u u_\alpha + B_w(L_g)v_{g\alpha} \tag{3}$$

being

$$A(L_g) = \begin{bmatrix} 0 & -\frac{1}{L_{c1}} & 0 \\ \frac{1}{C_f} & 0 & -\frac{1}{C_f} \\ 0 & \frac{1}{L_g} & 0 \end{bmatrix}, \; B_u = \begin{bmatrix} \frac{1}{L_{c1}} \\ 0 \\ 0 \end{bmatrix}, \; B_w(L_g) = \begin{bmatrix} 0 \\ 0 \\ -\frac{1}{L_g} \end{bmatrix}, \; x_\alpha = \begin{bmatrix} i_{c\alpha} \\ v_{c\alpha} \\ i_{g\alpha} \end{bmatrix} \tag{4}$$

where $i_{c\alpha}$ is the current in the inductor on the converter side, $v_{c\alpha}$ is the voltage in the filter capacitor and $i_{g\alpha}$ is the current in the inductor on the grid side, for axis α.

Since a model identical to (3)-(4) can be used for axis β, the subscripts α and β are suppressed from now on.

The parametric uncertainty on L_g can be taken into account by means of the polytopic representation

$$\dot{x} = A(\theta)x + B_u u + B_w(\theta)v_g \tag{5}$$

where

$$A(\theta) = \theta A_1 + (1-\theta)A_2, \;\; B_w(\theta) = \theta B_{w1} + (1-\theta)B_{w2} \tag{6}$$

and θ is a real parameter such that $0 \leq \theta \leq 1$.

In this representation, for instance, A_1 and A_2 are the vertices of the polytope, obtained by evaluating $A(L_g)$ for the minimum and maximum values of L_g.

For the application of a digital control strategy, consider the plant discretization with a sufficiently small sampling period T_s, leading to the discrete polytopic model

$$\begin{aligned} x(n+1) &= A_d(\theta)x(n) + B_{ud}(\theta)\;\varphi(n) + B_{wd}(\theta)v_g(n) \\ y(n) &= Cx(n) = [0\;0\;1]\;[i_c(n)\;v_c(n)\;i_g(n)]' \end{aligned} \tag{7}$$

where

$$A_d(\theta) = \theta A_{d1} + (1-\theta)A_{d2}\,, \qquad A_{di} = e^{A_i T_s} \tag{8}$$

$$B_{ud}(\theta) = \theta B_{ud1} + (1-\theta)B_{ud2}\,,\; B_{udi} = \int_0^{T_s} e^{A_i \tau} B_{ui} d\tau \tag{9}$$

$$B_{wd}(\theta) = \theta B_{wd1} + (1-\theta)B_{wd2}\,,\; B_{wdi} = \int_0^{T_s} e^{A_i \tau} B_{wi} d\tau \tag{10}$$

with $i = 1$ or $i = 2$, representing each one of the vertices.

The additional state

$$\varphi(n+1) = u(n) \tag{11}$$

is included to represent the transport delay in the control signal implementation [22].

Based on the internal model principle [23], to guarantee tracking of sinusoidal references and the rejection of harmonic disturbances, resonant controllers can be employed, being represented, in the continuous case, by

$$\begin{bmatrix} \dot{\delta}_r \\ \ddot{\delta}_r \end{bmatrix} = \overbrace{\begin{bmatrix} 0 & 1 \\ -\omega_n^2 & -2\xi\omega_n \end{bmatrix}}^{R_c} \begin{bmatrix} \delta_c \\ \dot{\delta}_c \end{bmatrix} + \overbrace{\begin{bmatrix} 0 \\ 1 \end{bmatrix}}^{T_c} e \tag{12}$$

where ω_n is the resonant frequency and ξ is the damping factor.

A discrete-time model of the resonant controller can be writen as [22]

$$x_r(n+1) = R_d\, x_r(n) + T_d\, e(n) \tag{13}$$

with

$$R_d = e^{R_c T s} \;\;, \;\; T_d = \int_0^{T_s} e^{R_c \tau} T_c d\tau \tag{14}$$

Generalizing, for ℓ independent resonant controllers, one has

$$R = \begin{bmatrix} R_{d1} & 0 & 0 & 0 \\ 0 & R_{d2} & 0 & 0 \\ 0 & 0 & \ddots & 0 \\ 0 & 0 & 0 & R_{d\ell} \end{bmatrix} \quad T = \begin{bmatrix} T_{d1} \\ T_{d2} \\ \vdots \\ T_{d\ell} \end{bmatrix} \tag{15}$$

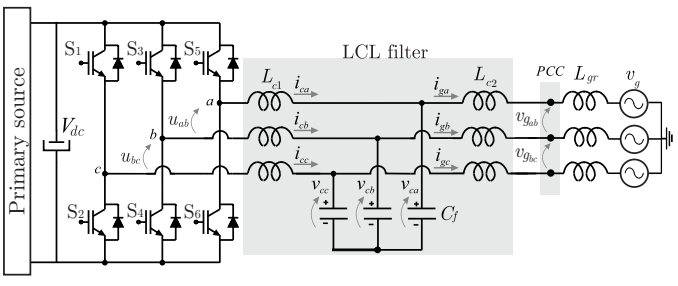

Figure 1. Three-phase grid connected inverter through LCL filter.

Finally, the augmented model can be written as

$$\begin{aligned}\rho(n+1) &= A_{aug}(\theta)\rho(n) + B_{uaug}u(n) \\ &\quad + B_{waug}(\theta)v_g(n) + B_{raug}r(n) \\ y(n) &= C_{aug}\rho(n)\end{aligned} \tag{16}$$

where $\rho(n) = [x(n)^{'}\ \varphi(n)\ \ x_r(n)^{'}]^{'}$ is the augmented state vector and

$$\begin{aligned}A_{aug}(\theta) &= \begin{bmatrix} A_d(\theta) & B_{ud}(\theta) & 0 \\ 0 & 0 & 0 \\ -TC & 0 & R \end{bmatrix}, B_{uaug} = \begin{bmatrix} 0 \\ 1 \\ 0 \end{bmatrix} \\ B_{waug}(\theta) &= \begin{bmatrix} B_{wd}(\theta) \\ 0 \\ 0 \end{bmatrix}, B_{raug} = \begin{bmatrix} 0 \\ 0 \\ T \end{bmatrix}\end{aligned} \tag{17}$$

This model is useful for the design of state feedback controller, and will be employed in the next section together with the PSO.

III. Control Design Procedure

Given the state space formulation of the problem in Section II, one can use the state feedback control law [22]

$$u(n) = K\rho(n) = \begin{bmatrix} K_x & K_\varphi & K_r \end{bmatrix} \begin{bmatrix} x(n) \\ \varphi(n) \\ x_r(n) \end{bmatrix} \tag{18}$$

where K is the vector of control gains.

In the proposed design procedure, the control gains will be obtained by means of a PSO algorithm, which requires an objective function to guide the optimization.

A. Objective function

The objective function has the purpose of measuring the system performance for a given control gain K. In the context of grid-tied inverters, the problem is to design robust control gains capable to ensure that the closed-loop grid currents track sinusoidal references even under disturbances and parameter uncertainties.

In order to achieve that, consider the proposed objective function

$$F(K) = \sigma(K)\gamma(K) + \frac{(380\sigma(K) - 360)}{1 + e^{-1000\sigma(K)+1000}} \tag{19}$$

In (19), the function $\sigma(K)$ provides a stability index evaluating the maximum module of the closed-loop system eigenvalues, defined by the maximum value of

$$\max |\lambda\left(A_{aug}(\theta) + B_{uaug}K\right)| \tag{20}$$

evaluated for $\theta = 0$ and $\theta = 1$, i.e., for the extreme values of L_g. It is known that evaluating the stability only at the vertices of a polytope is a necessary (but not sufficient) condition for the stability of the entire domain. However, it is used here since, from the computational point of view, this provides a simplified and fast way to approach the stability, which will be theoretically guaranteed by the LMI tests in the next section.

The function $\gamma(K)$ is a measure of the harmonic attenuation from the output PWM voltages to the current i_g, defined by the maximum value of

$$\max |C_{aug}(e^{j\omega T_s}I - (A_{aug}(\theta) + B_{uaug}K))^{-1}B_{uaug}| \tag{21}$$

evaluated for $\theta = 0$ and $\theta = 1$, over the frequency range $\omega \in \left[0,\ \frac{2\pi}{T_s}\right]$. These harmonics can be related with nonlinearities, as dead-time in the driving of the inverter switches, for instance.

Concerning the objective function, the first term of (19) allows to get a good trade-off between (20) and (21). However, evaluate only the first term may not guarantee that the solution is stable (i.e., $\sigma < 1$). For this, a second term is included to play the role of a penalization, using the sigmoid function. Thus, for unstable solutions, the value of the sigmoid function increases the objective function for higher values of σ. On the other hand, for values of $\sigma < 1$, the sigmoid function has almost zero value. In addition, the angular coefficient (equals to 380) and linear coefficient (equals to 360) are designed to increase the convergence of the solutions to the stable region.

The problem now is to find the robust control gain $K^\star$ that solves the following optimization:

$$K^\star = \arg\min_{K \in \mathcal{K}} F(K) \tag{22}$$

where $F(K)$ is given by (19), taking into account different controller candidates belonging to a search space $\mathcal{K}$, and (22) must be evaluated for $\theta = 0$ and $\theta = 1$.

The following subsection presents the PSO algorithm applied to the problem of finding robust control gains.

B. Particle swarm optimization

In order to use the PSO [14] in the control design problem above, consider that each vector K in (18) defines a particle position s_j (i.e., a point in a search space) with D dimensions, given by

$$s_j = [s_{j,1}\ \ s_{j,2}\ \ s_{j,3}\ \cdots\ s_{j,D}] \tag{23}$$

The algorithm initially creates a swarm of particles, randomly distributed in the search space. By evaluating the objective function, a fitness value is associated to the position of each particle. In successive iterations (called epochs) the positions are updated, and the swarm moves in the search space in order to find the minimum of the objective function.

For a given epoch m, a recursive velocity equation is used to update the position of each particle. The best position that each particle has ever obtained ($P_{j.best}$), and the best position among all particles (G_{best}) are defined by the objective function and the values are stored. The velocity and position recursive equations are given, respectively, by

$$v_j^{m+1} = \omega v_j^m + \eta_1 r_1(P_{j.best} - s_j^m) + \eta_2 r_2(G_{best} - s_j^m) \tag{24}$$

$$s_j^{m+1} = s_j^m + v_j^{m+1} \tag{25}$$

being η_1 e η_2 the cognitive and social coefficients, respectivelly, r_1 and r_2 random values between $[0, 1]$ and ω the inertia factor that decelerates the particles during the execution, for a better convergence.

The PSO execution used here has the following steps:

1) configure the PSO parameters;
2) initialize the particles randomly in the search space;
3) calculate the objective function for each particle;
4) update $P_{j.best}$ and G_{best};
5) update position and velocity of each particle;
6) if the stop criterion is reached, inform the best particle (G_{best}) and end the execution. If not, return to step 2.

At the end of the execution, the PSO algorithm returns the particle (i.e., the control gain $K^\star$) with the lowest objective function value associated (G_{best}). The number of particles, the number of epochs, and the coefficients η_1 and η_2 are set in order to ensure convergence of the objective function with viable computational effort.

After the PSO execution, a theoretical certificate of robust stability is provided, by means of LMIs, as can be seen in the next section.

IV. Robust Stability by means of LMIs

The control gain $K^\star$ provided by the PSO is obtained evaluating the closed-loop system stability and performance only for the vertices of the polytopic model. In order to provide a theoretical certificate of robust stability valid for the entire polytope, LMI based tests can be used, as follows.

The closed-loop system

$$\rho(n+1) = G(\theta)\rho(n) \tag{26}$$

with

$$G(\theta) = A_{aug}(\theta) + B_{uaug}(\theta)K \tag{27}$$

is stable for all $0 \leq \theta \leq 1$ if there exist symmetric positive matrices P_1 and P_2 such that

$$G_1^{'}P_1G_1 - P_1 < -I, \quad G_2^{'}P_2G_2 - P_2 < -I \tag{28}$$

and

$$\begin{aligned} &G_1^{'}P_1G_2 + G_2^{'}P_1G_1 + G_1^{'}P_2G_1 - 2P_1 - P_2 < I, \\ &G_2^{'}P_2G_1 + G_1^{'}P_2G_2 + G_2^{'}P_1G_2 - 2P_2 - P_1 < I \end{aligned} \tag{29}$$

The proof can be found in [24] for the general case of N vertices, and was specialized here for 2 vertices. The results with the above LMIs are less conservative than the well known quadratic stability [20], allowing to get theoretical certificates of robust stability even when the quadratic stability fails.

V. Case Study and Experimental Validation

As a case study, consider the GTI shown in Figure 1, with parameters given in Table I. Note that there are 4 resonant controllers, which lead to a x_r vector with 8 states, that, together with the 3 states of x and the state ϕ, results in an augmented state vector of 12 states.

The PSO parameters are chosen as: 50 particles, 200 epochs and $\eta_1 = \eta_2 = 0.5$. For each entry of K, the limits that defines the search space are given in Table II. These values were obtained from a digital linear quadratic regulator control vector, tuned with Q being the identity matrix and $R = 1$.

Table I
GTI Parameters.

Parameters	Values
L_{c1}, C_f and L_{c2}	1 mH, 62 μF and 0.3 mH
L_g	[0, 1] mH
DC-link voltage V_{dc}	400 V
Grid voltage v_g	180 V (peak); 60 Hz
Sampling frequency	20040 Hz
Switching frequency	10020 Hz
Frequencies of resonant controllers	60, 180, 300 and 420 Hz
Damping factor	0.0001

Table II
Search space $\mathcal{K}$ limits for the GCC case study.

s_j	$s_{j,1}$	$s_{j,2}$	$s_{j,3}$	$s_{j,4}$	$s_{j,5}$	$s_{j,6}$	$s_{j,7}$	$s_{j,8}$	$s_{j,9}$	$s_{j,10}$	$s_{j,11}$	$s_{j,12}$
s_{jmin}	-15	-15	-15	-15	0	-100	0	-50	0	-50	0	-50
s_{jmax}	0	0	0	0	100	0	50	0	50	0	50	0

The PSO was executed several times, always converging to viable controllers. After a typical execution, the PSO led to the solution

$$\begin{aligned} K^\star = [&-9.6783 \;\; -2.1732 \;\; -1.2914 \;\; -0.2858 \\ &73.7784 \;\; -73.7457 \;\; 18.1096 \;\; -17.6463 \\ &23.0582 \;\; -23.4587 \;\; 23.0796 \;\; -23.8390] \end{aligned} \tag{30}$$

for which the fitness has the evolution shown in Figure 2(a).

Evaluating functions (20) and (21) for the gain (30) one has $\sigma = 0.9933$ and $\gamma = 0.3109$. The value of σ can be confirmed by the eigenvalues location in the unit circle, shown in Figure 2(b), for a sweep in L_g from 0 mH to 1 mH. The value of γ can be confirmed by the frequency response of model (16) from the input u to the output i_g, shown in Figure 3, confirming rejection of disturbances for all frequencies, specially in the harmonics of the resonant controller, which also ensure good rejection of harmonics from the grid voltages, which was confirmed by time-simulations.

When verifying the feasibility of the LMIs (28) and (29) with the control gain (30), the LMI Control Toolbox from Matlab confirm that there exist symmetric positive matrices P_1 and P_2 solving the problem, which theoretically certifies the stability for the entire domain of uncertain parameters (i.e., for L_g assuming any value from L_{gmin} to L_{gmax}).

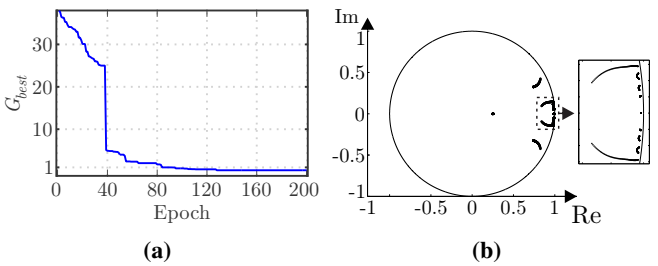

Figure 2. (a) Evolution of G_{best} in each epoch; (b) Closed-loop eigenvalues for a sweep in L_g, confirming the value $\sigma = 0.9933$.

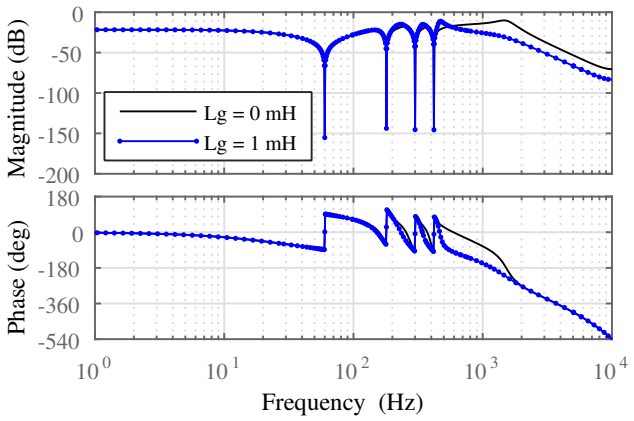

Figure 3. Frequency response from u to ig, for the extreme values of L_g, confirming the value $\gamma = 0.3109$ (i.e. -10.15 dB).

A. Experimental Results

To evaluate the system performance with control gains in (30), experimental results are obtained with a 5.4 kW prototype. The prototype is comprised by a three-phase inverter based on IGBTs and a three-phase LCL filter, with system parameters in Table I. Filter states (currents and voltages) are measured using Hall effect sensors. The control law is synthesized in a DSP TMS320F28335 and the grid synchronization with the PCC is provided by a Kalman filter algorithm [25].

Figure 4 shows the grid-injected currents, in α and β axes, under reference amplitude variations for the converter connected to a real utility grid. The first variation represents the start-up of the system, injecting active power into the grid, while the second one represents an increase in the current amplitude to 20 A. From these results it is possible to verify that the system is capable of tracking sinusoidal grid-current references with suitable steady-state and transient responses.

The three-phase currents related to the test performed in Figure 4 are shown in Figure 5 (a), and the transient responses are detailed in Figure 5 (b) and (c), highlighting the overall good closed-loop performance.

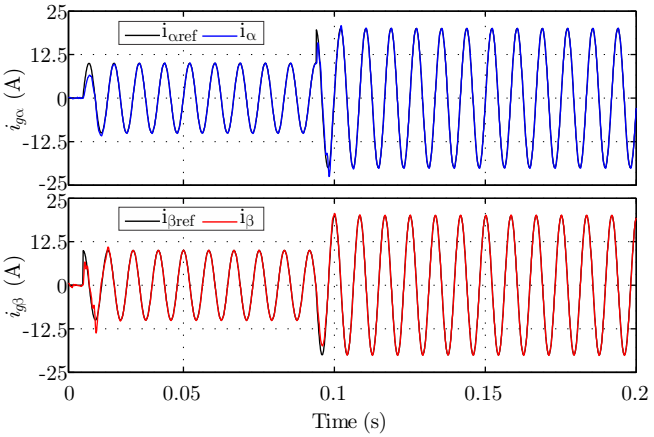

Figure 4. Experimental grid-injected currents in α axis (top) and β axis (bottom) for an experimental test under reference variations (data from DSP).

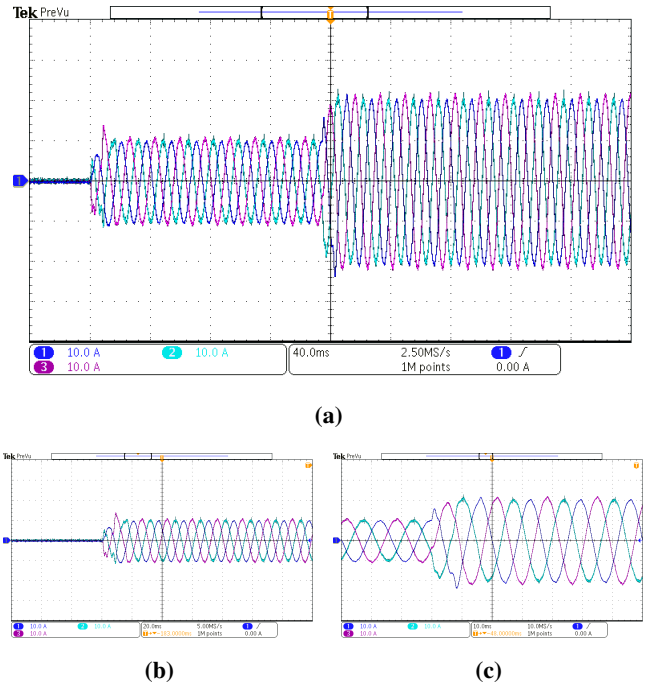

Figure 5. Experimental three-phase grid currents for the reference variations in Figure 4 (vertical scale: 10 A/div): (a) full test; (b) converter start-up; (c) increase in the active power.

Figure 6 (a) shows the three-phase grid currents in steady-state. For one of the phases, the harmonic spectrum is given in Figure 6 (b), showing that the closed-loop system with control gain (30) is able to properly synthesize grid currents with individual harmonic components that comply with the limits from the IEEE 1547 Standard, and with total harmonic distortion less than 5%, also complying with this Standard.

Finally, to evaluate the closed-loop stability under uncertain grid inductances, a test is performed with the filter disconnected of the PCC. A short-circuit is then applied to the output of the filter, and the grid inductance is emulated with additional inductors, included in series with L_{c2}. Figure 7 (a) and (b) shows the system start-up with L_{gmin} (i.e. $L_g = 0$ mH) and L_{gmax} (i.e. $L_g = 1$ mH), respectively. It is possible to confirm

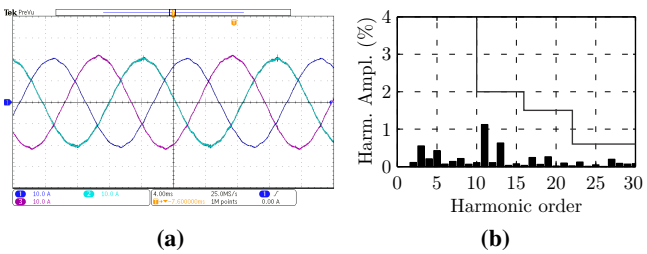

Figure 6. Experimental results for harmonic content analyses (vertical scale: 10 A/div): (a) Steady-state currents; (b) harmonic spectrum and limits from IEEE 1547 Standard.

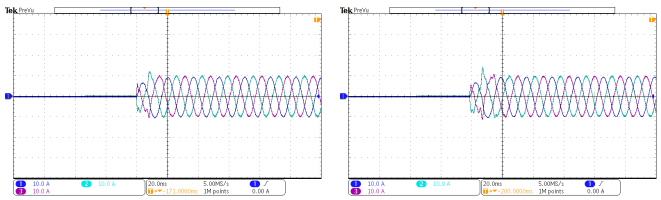

(a) **(b)**

Figure 7. Experimental results for stability evaluation under uncertain parameter (vertical scale: 10 A/div): three-phase grid currents for an off-grid test emulating (a) L_{gmin} and (b) L_{gmax}.

the stability under uncertain parameters, ensured by the LMIs, with suitable transient and steady-state responses.

ACKNOWLEDGMENTS

This study was financed in part by the Coordenação de Aperfeiçoamento de Pessoal de Nível Superior - Brasil (CAPES/PROEX) - Finance Code 001. The authors would also like to thank the INCT-GD and the finance agencies (CNPq 465640/2014-1, CNPq 309536/2018-9, CAPES 23038.000776/2017-54 and FAPERGS 17/2551-0000517-1).

VI. CONCLUSION

This paper provides an automatic procedure for the design of robust state feedback current controllers for GTIs, leading to grid-injected currents in compliance with requirements from IEEE 1547 Standard. The design is based on a PSO, which searches the control gains guided by the minimization of an objective function that takes into account a trade-off between the settling of transient responses and disturbance rejection. Differently of other papers, LMIs are used to theoretically certify the robust stability of the closed-loop for the entire interval of grid uncertain inductances. Experimental results are shown, confirming compliance of the steady-state responses with requirements from IEEE 1547 Standard for individual harmonics and total harmonic distortion, and also suitable transient recovers.

REFERENCES

[1] R. Teodorescu, M. Liserre, and P. Rodríguez, *Grid Converters for Photovoltaic and Wind Power Systems*, ser. Wiley - IEEE. John Wiley & Sons, 2011.

[2] F. Blaabjerg and K. Ma, "Future on power electronics for wind turbine systems," *IEEE Journal of Emerging and Selected Topics in Power Electronics*, vol. 1, no. 3, pp. 139–152, Sep. 2013.

[3] F. Blaabjerg, R. Teodorescu, M. Liserre, and A. Timbus, "Overview of control and grid synchronization for distributed power generation systems," *IEEE Transactions on Industrial Electronics*, vol. 53, no. 5, pp. 1398 –1409, oct. 2006.

[4] C. Poongothai and K. Vasudevan, "Design oflclfilter for grid-interfaced pv system based on cost minimization," *IEEE Transactions on Industry Applications*, vol. 55, no. 1, pp. 584–592, Jan 2019.

[5] *IEEE:1547 Standard for interconnecting distributed resources with electric power systems*, Institute of Electrical and Electronics Engineers Std., 2011.

[6] I. Gabe, V. F. Montagner, and H. Pinheiro, "Design and implementation of a robust current controller for VSI connected to the grid through an LCL filter," *IEEE Transactions on Power Electronics*, vol. 24, no. 6, pp. 1444–1452, June 2009.

[7] M. Lu, A. Al-Durra, S. M. Muyeen, S. Leng, P. C. Loh, and F. Blaabjerg, "Benchmarking of stability and robustness against grid impedance variation forlcl-filtered grid-interfacing inverters," *IEEE Transactions on Power Electronics*, vol. 33, no. 10, pp. 9033–9046, Oct 2018.

[8] J. Dannehl, F. W. Fuchs, S. Hansen, and P. B. Thogersen, "Investigation of active damping approaches for PI-based current control of grid-connected pulse width modulation converters with LCL filters," *IEEE Transactions on Industry Applications*, vol. 46, no. 4, pp. 1509–1517, July 2010.

[9] R. Teodorescu, F. Blaabjerg, M. Liserre, and P. Loh, "Proportional-resonant controllers and filters for grid-connected voltage-source converters," *IEE Proceedings Electric Power Applications*, vol. 153, no. 5, pp. 750–762, September 2006.

[10] L. A. Maccari, Jr., J. R. Massing, L. Schuch, C. Rech, H. Pinheiro, R. C. L. F. Oliveira, and V. F. Montagner, "LMI-based control for grid-connected converters with LCL filters under uncertain parameters," *IEEE Transactions on Power Electronics*, vol. 29, no. 7, pp. 3776–3785, July 2014.

[11] G. G. Koch, L. A. Maccari, R. Oliveira, and V. F. Montagner, "Robust $\mathcal{H}_\infty$ state feedback controllers based on lmis applied to grid-connected converters," *IEEE Transactions on Industrial Electronics*, pp. 1–1, 2018.

[12] C. R. D. Osório, G. G. Koch, H. Pinheiro, R. C. L. F. Oliveira, and V. F. Montagner, "Robust current control of grid-tied inverters affected by lcl filter soft-saturation," *IEEE Transactions on Industrial Electronics*, pp. 1–1, 2019.

[13] S. E. De León-Aldaco, H. Calleja, and J. A. Alquicira, "Metaheuristic optimization methods applied to power converters: A review," *IEEE Transactions on Power Electronics*, vol. 30, no. 12, pp. 6791–6803, 2015.

[14] R. Eberhart and J. Kennedy, "A new optimizer using particle swarm theory," in *Micro Machine and Human Science, 1995. MHS'95., Proceedings of the Sixth International Symposium on*. IEEE, 1995, pp. 39–43.

[15] B. Ufnalski, A. Kaszewski, and L. M. Grzesiak, "Particle swarm optimization of the multioscillatory LQR for a three-phase four-wire voltage-source inverter with an LC output filter," *IEEE Transactions on Industrial Electronics*, vol. 62, no. 1, pp. 484–493, 2015.

[16] A. Murari, L. Rodrigues, J. Altuna, A. S. Potts, L. Almeira, and A. Sguarezi Filho, "A LQRI power control for DFIG tuned by a weighted-PSO," *Control Engineering Practice*, vol. 85, pp. 41–49, 2019.

[17] A. Zobaa and A. Lecci, "Particle swarm optimisation of resonant controller parameters for power converters," *IET power electronics*, vol. 4, no. 2, pp. 235–241, 2011.

[18] S. S. Sebtahmadi, H. B. Azad, S. H. A. Kaboli, M. D. Islam, and S. Mekhilef, "A PSO–DQ current control scheme for performance enhancement of Z–source matrix converter to drive IM fed by abnormal voltage," *IEEE Transactions on Power Electronics*, vol. 33, no. 2, pp. 1666–1681, 2017.

[19] Z.-L. Gaing, "A particle swarm optimization approach for optimum design of PID controller in AVR system," *IEEE transactions on energy conversion*, vol. 19, no. 2, pp. 384–391, 2004.

[20] S. Boyd, L. El Ghaoui, E. Feron, and V. Balakrishnan, *Linear Matrix Inequalities in System and Control Theory*. Philadelphia, PA: SIAM Studies in Applied Mathematics, 1994.

[21] L. A. Maccari, A. C. L. Santini, H. Pinheiro, R. C. L. F. de Oliveira, and V. F. Montagner, "Robust optimal current control for grid-connected three-phase pulse-width modulated converters," *IET, Power Electronics*, vol. 8, no. 8, pp. 1490–1499, 2015.

[22] K. Ogata, *Discrete-time control systems*. Prentice Hall, 1995.

[23] B. A. Francis, *A Course in $\mathcal{H}_\infty$ Control Theory*, ser. Lectures Notes in Control and Information Sciences. New York: Springer-Verlag, 1987, vol. 88.

[24] D. C. W. Ramos and P. L. D. Peres, "A less conservative LMI condition for the robust stability of discrete-time uncertain systems," *Systems & Control Letters*, vol. 43, no. 5, pp. 371–378, August 2001.

[25] R. Cardoso, R. F. de Camargo, H. Pinheiro, and H. A. Gründling, "Kalman filter based synchronisation methods," *Generation, Transmission Distribution, IET*, vol. 2, no. 4, pp. 542–555, july 2008.

Robust State Observers Design Based on LMIs Applied to Grid-Connected Converters

***Abstract*—This paper provides a procedure to design robust state observers applied to the control of three-phase inverters with LCL filters connected to the grid with uncertain and time-varying impedances. Linear matrix inequalities, are used to compute offline a set of fixed observer gains and to provide an upper bound for the rate of grid impedance variations for which the closed-loop stability is guaranteed, based on Lyapunov functions. The proposed procedure allows implementing robust state feedback controllers with a reduced number of sensors, keeping stability and good performance under parametric variations, as confirmed by the experimental results. The control law using the observed states can ensure grid currents with low harmonic content, complying with the IEEE 1547 Standard requirements, with negligible loss of performance with respect to the feedback of the measured state variables. Four different robust state feedback controllers from the literature are implemented with the robust state observer designed by means of the proposed procedure, allowing suitable performances in all cases, confirming the viability of the proposal.**

***Index Terms*—Grid-connected converters, Linear matrix inequalities, State observers, Uncertain parameters.**

I. Introduction

The presence of renewable sources is a central issue for electrical energy generation in a sustainable way, and the inverters are important systems to control the power flow between these sources and the mains [1], [2]. Moreover, the currents injected into the grid must comply with limits for harmonic distortion and, for these purpose, LCL filters are widely used as output stage of the inverters [3], [4]. However, these filters present a resonance peak that usually demand damping, which is more challenging considering the need to ensure stability and performance for systems subject to uncertain parameters [5]-[7]. In this context, an important alternative for active damping is the state feedback control strategy, able to provide a good tradeoff between robustness and performance for this application [8]-[11].

A recognized tool to design robust state feedback controllers in an systematic and efficient way are the linear matrix inequalities (LMIs) [12]. Considering LCL filter applications, LMIs have been successfully applied for robust control design, for instance, in [13]-[15]. On the other hand, although full-state feedback techniques can ensure stability and suitable results, they rely on the knowledge of all LCL filter state variables, which can represent an increase in cost of implementation if additional sensors are required. To avoid that, state observers are an interesting tool, allowing to implement state feedback control strategies with a reduced number of sensors [16], [17].

State observers were employed for three-phase LCL filter applications, for instance, in [18]-[21]. In [18], considering that all system parameters are precisely, known, a state observer is used to predict the filter capacitor current used to active damp the LCL resonance. In [19], it is proposed an analytical method for discrete-time design of an observer-based state-space current control in synchronous reference frame. The designs of both controller and observer are carried out separately, by means of direct pole placement, without taking into account uncertain parameters. The parameter sensitivity is analyzed afterwards, based on the Nyquist criterion. In [20], an observer-based control with fixed gains is designed for operation varying from strong to weak grid conditions. Intervals for the choice of the control parameters are obtained, but assessing the robustness by testing the closed-loop system eigenvalues using exhaustive discretization. In [21], an observer is used to control the grid-side current by only measuring the converter-side currents and the grid-side voltage. The control is also performed in synchronous reference and the robustness against uncertain parameters is demonstrated *a posteriori*, based on the analysis of results.

The design of observer-based controllers is challenging especially when dealing with uncertain and possibly time-varying parameters, since the mismatches between the models and the actual plant parameters can degrade the dynamic responses of the closed-loop system. Additional strategies may be required to ensure closed-loop stability and compliance with performance constraints for the entire range of parametric variations. In this scenario, conditions based on LMIs for the design of observers were presented in [22] and [23], for linear systems with state-space matrices affected by parametric uncertainties, but only in the continuous-time domain. In [24], it is proposed a design of robust state observers, based on LMIs, for discrete-time polytopic systems. Nevertheless, in these LMI based works, the problems of reference tracking and rejection of sinusoidal disturbances are not addressed, and the delay on the implementation of the control signal is not included in the model. In this direction, in [25] it is presented a procedure to design a state observer-based robust controller for an LCL filter connected to a grid with uncertain parameters, including formulation in the discrete-time domain and taking into account the implementation delay. However, only evaluations for time-invariant parameters were presented, for a single-phase inverter, with no experimental validation and without coping with parameters varying on time.

The main objective of this paper is to provide a procedure to design fixed gains of a robust state observer for three-phase LCL-filtered grid-connected converters, suitable for practical applications with a reduced number of sensors. Differently from previous works, the proposed design leads to an observer-based current control that ensures robustness in the scenario of time-varying grid inductances, thanks to the use of LMIs